Master Thesis in Geographical Information Science nr 156

Impact of Sea Surface Temperature and Salinity on Phytoplankton blooms phenology in the North Sea

Krystyna Muszel

2023
Department of
Physical Geography and Ecosystem Science
Centre for Geographical Information Systems
Lund University
Sölvegatan 12
S-223 62 Lund
Sweden

Krystyna Muszel (2023). Impact of Sea Surface Temperature and Salinity on Phytoplankton blooms phenology in the North Sea

Master degree thesis, 30 ECTS credits in Master in Geographical Information Science

Department of Physical Geography and Ecosystem Science, Lund University

Impact of Sea Surface Temperature and Salinity on Phytoplankton blooms phenology in the North Sea

---

By Krystyna Muszel, 2023

Master thesis, 30 credits, in Geographical Information Sciences
Lund University, Sweden

Supervisor:

Dr Marko Scholze

Department of Physical Geography and Ecosystem Science
Lund University, Sweden

Abstract

Various environmental forcings can affect phytoplankton blooms, resulting in changes in bloom timing and abundance, which can have many far-reaching consequences. Understanding bloom phenology is crucial to predict and counter any potential harmful changes. The North Sea is an important fishing ground, and any changes in phytoplankton bloom patterns can have a significant impact on the region's economy. The aim of this thesis was to assess interannual and long-term changes in the timing and abundance of phytoplankton blooms in the North Sea, and to determine if Sea Surface Temperature (SST) and Sea Surface Salinity (SSS), as a proxy for nutrients, can explain the variability of those parameters. Merged satellite data from 4 sensors: SeaWiFS, MERIS, MODIS AQUA and VIIRS were used to evaluate bloom patterns, using the chlorophyll-a concentration between 2002 and 2020 (except 2017) inside TIMESAT software. Due to satellite data limitations, it was possible to survey only spring bloom, as the data is not available year-round.

There was no evident change in the spring bloom timing over the studied period. The chl-a maximum concentration values decreased over time, with statistically significant results for the region A, along the Scottish coast (Pearson $r=-0.75$, $p<0.001$) and region F, between the coast of Denmark, Germany, and the Netherlands ($r=-0.68$, $p<0.05$). The southern region (region E) was an exception from the general pattern and showed an increase of the chlorophyll-a concentration during the investigated years ($r=0.47$, $p<0.05$). SST showed a medium correlation with chl-a data ($r=0.54$, $p<0.001$), but it did not explain the fluctuations of the peak values of chl-a in specific regions, proving the need to take into consideration local environmental processes. SSS showed only a negative correlation with bloom parameters in the Dogger Bank region (region D) explaining the bloom timing fluctuations. Higher salinity correlated with a faster start of bloom ($r=-0.60$, $r=-049$ with a $p<0.05$ for salinity in summer and in winter respectively) and faster peak time ($r=-055$, $p<0.05$ for salinity in summer).

In conclusion, this study presents a further insight to spring phytoplankton bloom timing and bloom intensity in the North Sea. The phytoplankton bloom trends differed across the study area and could not be explained only by the SST and SSS. This variability in bloom parameters proves that other local environmental factors need to be considered to understand better which processes influence the bloom phenology.

Keywords: Geography, GIS, North Sea, phytoplankton, bloom, phenology, remote sensing, TIMESAT software

TABLE OF CONTENTS

1. Introduction

1.1 Knowledge gap

Phytoplankton blooms in the North Sea have previously been studied and the mechanisms of bloom formation are well understood in this region. However, regardless of the extensive research already performed, investigating variability in the bloom patterns, and understanding which environmental factors determine the timings and intensity of the bloom in this region is still needed. Understanding phytoplankton blooms is important because phytoplankton form the basis of the marine food chain, and all marine life depends on them. Higher trophic levels can be influenced by interannual blooms variability. Additionally, potential changes in long-term trends in bloom timing, length and intensity could have significant long-term consequences for marine organisms and the economy of this region.

The shallow waters in the south of the North Sea are influenced by proximity of the continent and characterize by high riverine inflow. Contrarily, the north of the North Sea has deeper waters that are affected by the proximity of the Atlantic Ocean. Phytoplankton blooms in both areas are triggered in different ways. Moreover, different factors and their relationships make the investigation of bloom pattern fluctuations and trends due to climate change in this region complex. Sea Surface Temperature (SST) and Sea Surface Salinity (SSS), which was used as an indicator for nutrients, are dependent on North Atlantic Oscillation Index (van Beusekom, J. E., & Diel-Christiansen, S, 2009) and both were under investigation as potential factors that could explain phytoplankton bloom variations.

Despite previous studies (Alvarez-Fernandez, S. et al., 2012, Opdal, A. F., et al., 2019, Desmit, X., et al., 2020) into factors that could influence a shift in bloom onset in the North Sea, trends in other parameters of bloom phenology and what environmental variables may influence them need to be better understood. At the research stage and during analysis, no other papers had been found that investigated them in the North Sea. However, a recent study by Silva, E., et al., (2021) that was written simultaneously with this master thesis also consider and analyse such parameters, however the method used differed from the methodology of this work. To the best of knowledge, this thesis was the first to investigate if TIMESAT software could be used to

evaluate the phytoplankton bloom using remote sensed chlorophyll-a (chl-a) data in the North Sea.

1.2 Aims and hypothesis

The aim of this thesis is to investigate the long-term trends in the onset, peak day, peak value, end, and length of phytoplankton blooms in the North Sea and assess whether there is a shift in the bloom timing, changes in the duration or maximum chl-a concentration using ocean colour remote sensing data. The environmental variables, sea surface temperature and salinity as a proxy for nutrients, were investigated to determine if they could explain the variability of those parameters. It is hypothesized that the spring bloom season will occur earlier in the year and have an earlier peak day. The second season is theorized to finish later in the year. This may elongate the duration of the phytoplankton bloom phenomenon in both bloom seasons. It is also presumed that the earlier spring bloom and later end of late spring/early autumn bloom could be explained by higher SST and higher SSS in the open waters or lower SSS in the areas influenced by riverine inflow. Additionally, higher SST and higher SSS in the open waters, or lower SSS in the areas influenced by riverine inflow, will cause chl-a concentration to reach higher maximum values. The North Sea phytoplankton phenology trends and potential correlations with SST and SSS were investigated for the whole sea and for 6 regions separately to gain more insight into regions with unique characteristics. The period of 1998-2020, excluding the year 2017, was analysed using merged satellite data.

2. Background and theory

2.1 Description of phytoplankton organisms and how to measure their abundance

Plankton are often described as organisms that do not have the ability to move and can only drift in the water (Pachiappan, P., et. al 2019), however, exceptions exist as some species can move slightly vertically in the water column (Wirtz, K., & Smith, S. L., 2020). The plankton group is divided into phytoplankton, which is a collective of photosynthetic organisms, and animal plankton called zooplankton (Reynolds, C. S., 2006). Plankton can be divided into classes depending on their size from the largest ones that can reach even 2m (for example, large jellyfish) to very tiny viruses that can be as small as 0.02 μm (Garrison, T. S., 2012).

Research on plankton organisms has been conducted since the first half of the XIX century (Reynolds, C. S., 2006). Johannes Müller, a German physiologist, anatomist, and zoologist demonstrated them to his students in the 1840s, calling them *Auftrieb* which translates to "up drive" (Reynolds, C. S., 2006). Later, one of his pupils, Ernst Haeckel, expanded the knowledge of the different plankton forms. In the second part of the XIX century, Victor Hansen started using quantitative methods to study these microscopic organisms (Reynolds, C. S., 2006). He was the first person to call them *Plankton* from the Greek word for "wandering" in the year 1887 (Santhanam, P. et. al 2019). Hansen studied the North Sea fish stock and discovered that phytoplankton are an important food source, not only for fish, but also copepods and other small animals, and that it needs light to grow. The first major plankton research expedition took place on the *Meteor* science vessel in 1925 (Garrison, T. S., 2012). The techniques used during this expedition, such as the use of plankton nets, are still in practice. Plankton nets are usually made from nylon to allow the water to pass through but keep the planktonic organisms in.

Phytoplankton are considered one of the most vital primary producers on Earth. There are approximately 20 000 phytoplankton species that can be divided into at least 8 types (Falkowski, P. G., et al. 2003). The most well-known are cyanobacteria, diatoms, dinoflagellates, green algae and coccolithophores, with diatoms being considered as the most abundant and having the highest productivity (Garrison, T. S., 2012). However, in the 1980s, researchers started to study picoplankton organisms that are less than 2 μm in size and are represented by numerous cyanobacteria species. These studies indicate that picoplankton may

be responsible for much greater primary production than previously thought (Garrison, T. S., 2012).

All phytoplankton organisms contain chlorophyll in their cells, a pigment which absorbs light at specific wavelengths. Depending on the species, phytoplankton can hold various kinds of chlorophyll (Reynolds, C. S., 2006) and other colour pigments. Chlorophyll-a (chl-a) is found in all phytoplankton organisms and its concentration is widely used as a proxy for determining phytoplankton biomass (Siswanto, E. 2020). Although chl-a correlates well with phytoplankton biomass, it is worth noting that chl-a per unit of phytoplankton biomass can vary between species, which can lead to uncertainty in the results (Wasmund, N., et al. 2019).
Chl-a measurements are a common technique used to study phytoplankton organisms. Presently, new in situ methods have been developed that allow for surveying chl-a in the deeper parts of the water by using submersible in situ fluorometers (Leeuw, T., et al. 2013). On-site surveys can supply mostly correct data, but the information is only available locally and it cannot be accessed daily. Monitoring became easier when satellites that could measure ocean colour products became active. In 1978, the first satellite with a sensor on board that could do that, the Coastal Zone Color Scanner (CZCS), was launched. Since that event, other satellite sensors have been made available to measure ocean colour, including chl-a concentration.

Chl-a absorbs light in the blue and red spectrum with the maximum peak of approximately 430nm and 675nm and is responsible for the colour of the water. Chl-a concentration data has been available continuously since 1997, when the SeaWiFS sensor began supplying ocean reflectance data. Satellite or aerial imageries allow for greater coverage than in situ surveys, however, they have limitations. They can measure chl-a just in the upper layer of the water and can be used for collecting chl-a data only during daylight and only if clouds are not present. Furthermore, the satellite-derived data in coastal waters are problematic. In coastal zones the optical properties are more complex due to presence of non-phytoplankton Coloured Dissolved Organic Matter (CDOM) and other inorganic suspended matters in the waters due to higher turbidity (Eleveld, M. A., et al., 2007, Gohin, F., et al. 2020). Various local algorithms have been developed to produce more accurate results of the chl-a concentration. The in-situ data is treated as ground truth and it is used for calibration of those algorithms; however, even the in-situ measurements can be uncertain. Fluorimetry measurements can underestimate or overestimate the presence of chl-a (Gohin, F., et al. 2020).

2.2 Importance of phytoplankton organisms

Phytoplankton play a vital role in the marine ecosystem. It is a primary producer, meaning its blooms are the base of the marine food web. It transports the biomass and energy to higher trophic levels, firstly to herbivorous zooplankton, then carnivorous zooplankton, gelatinous zooplankton, fish, seabirds, and finally marine mammals. Without phytoplankton other marine organisms would not be able to exist.

Like terrestrial plants, phytoplankton convert carbon dioxide and water into organic carbon and oxygen during the photosynthesis process. According to scientists, at least 50% to even 80% of the oxygen produced on Earth comes from the ocean, and phytoplankton are responsible for the majority of its production (NOAA, 2021). Furthermore, phytoplankton plays a key role in the movement of carbon in the ocean biological pump. It moves organic carbon up the food chain by being consumed by other marine life forms. If phytoplankton are not consumed and they die, they decay and sink to the deep ocean to finally decompose, trapping carbon in sediments for prolonged periods of time, up to millions of years, hence removing the carbon dioxide from the atmosphere. This means that phytoplankton are important organisms in the blue carbon ecosystem (Siswanto, E., 2020) which annually transport tens of gigatons of carbon to the deep ocean (Santhanam, P., 2019).

2.3 Phytoplankton requirements to trigger a bloom

To flourish, phytoplankton need specific conditions. When nutrients and sunlight availability are favourable to sustain growth, phytoplankton will multiply rapidly, and a phenomenon known as a phytoplankton bloom will occur (Garrison, T. S., 2012). Carbon dioxide, oxygen, and other nutrients such as nitrogen, phosphorus, silicate, and calcium are needed to trigger growth. The exact nutrient requirements are dependent on the species of phytoplankton present (Barcelos e Ramos, J. et al. 2017).

Phytoplankton blooming can be hindered in situations where not all of the nutrients are contained in the water column. For example, insufficient silicate can limit the blooms of diatoms (Riebesell, U., & Wolf-Gladrow, D. A., 2002) which need it to build their cell walls. In the central part of the North Sea, nitrogen is the limiting factor, and its deficiency ends the

first bloom, while in coastal areas commonly phosphate and silicate deplete the fastest, limiting the growth (Quante, M., et al. 2016). When other trace elements required by the phytoplankton are scarce, they can lessen primary production (Riebesell, U., & Wolf-Gladrow, D. A., 2002). One of the examples of trace elements that can have a limiting impact on blooms is the iron (Tilman, D., et al. 1982) that is needed for phytoplankton to maintain the metabolic processes (Garrison, T. S., 2012).

The second condition that needs to be fulfilled for the bloom to occur is the sufficient light availability that is needed for the process of photosynthesis during which the photosynthetically active radiation (PAR) is converted into chemical energy. Assimilation pigments, like chlorophyll, handle the absorption of light, which is used to produce glucose and, as a by-product, oxygen from carbon dioxide and water, leading to the growth of the phytoplankton (Garrison, T. S., 2012). The peak of the bloom happens when there is plentiful light and nutrients to support high productivity (Garrison, T. S., 2012). The bloom ends when the nutrients are depleted. This phenomenon does not last exceptionally long, from a few weeks to a few months.

During the bloom the highest productivity will occur close to the surface in the top layer of the water where there is plentiful light (Garrison, T. S., 2012). However, too much light could also impede the bloom (Garrison, T. S., 2012). Additionally, in deeper layers, lower light availability will inhibit the photosynthesis process and decrease productivity. The depths where phytoplankton respiration requires all the produced, during the photosynthesis process, glucose and oxygen, is called compensation depth. Compensation depth varies depending on the phytoplankton species and other environmental constraints that are responsible for the amount of light that reaches the deeper waters (Garrison, T. S., 2012). Phytoplankton that sink below the compensation depth are not able to grow, and if the light conditions do not improve, they will consume their reserves and finally die.

Algal biomass in the North Sea consists mainly of phytoplankton (Reid, P. C et al., 1990). It is a region where typically two blooms occur, one in spring and the second in late summer or early autumn (Quante, M., et al. 2016). Those blooms start due to different physical forcings (Martinez, E., et al. 2011). The spring bloom starts when more sunlight reaches the water surface allowing for better light penetration of the water column. During this time waters contain plentiful nutrients after winter deep mixing caused by intense winds. In this period in

the central and northern North Sea, the stratification occurs with a strong thermocline forming in May (Quante, M., et al. 2016) which keeps the nutrients close to the surface letting the photosynthesis process accelerate and the phytoplankton biomass to explode. On the other hand, in the Skagerrak strait, the bloom occurrence relates to the inflow of Baltic Sea waters that have a much lower salinity and initiate the haline stratification (McQuatters-Gollop, et al. 2007) that, similarly to thermocline, will trap nutrients close to the surface.

The situation is different in the shallow south part of the North Sea where the water is well mixed all year due to tidal currents (Quante, M., et al. 2016). Those currents mix the waters horizontally and vertically, hence bringing waters rich in nutrients to the surface. Consequently, in those regions' blooms are mostly controlled by light availability. The key factors that can limit the blooms in the south are the suspended matter in water column that decreases in the spring when the intense winds subside and cloudiness that can lessen the light penetration (McQuatters-Gollop, et al. 2007). Nevertheless, spring blooms in the south and north are abundant and account for most of the North Sea primary production (Quante, M., et al. 2016). Those blooms consist mostly of diatoms (McQuatters-Gollop, et al. 2007). The reasons for the end of spring bloom are nutrient deficiencies and zooplankton grazing by copepods, which consume about 10% to 20% of phytoplankton in coastal waters (Quante, M., et al. 2016).

In late summer or early autumn, a bloom is triggered when the depleted surface waters are again replenished with nutrients. In open waters, powerful winds allow for enhanced vertical mixing. The water column is destabilized. The stratification breaks up, which brings waters rich in nutrients from a deeper part of the sea to the well-lighted, depleted surface waters through upwelling. In the case of coastal waters, the main driver of new nutrients is river runoff. During the second bloom dinoflagellates, which are adapted to survive in nutrient-poor waters (McQuatters-Gollop, et al. 2007), are the most common phytoplankton (Quante, M., et al. 2016). Diatoms may also bloom during late summer or early autumn, although this bloom would be less abundant than in the spring (Quante, M., et al. 2016).

2.4 Factors influencing the blooms and related risks.

Detecting the long trend in phytoplankton phenology and magnitude of blooms is complex due to large interannual, spatial and temporal differences. Climate variability, land-ocean

interactions in coastal waters and other environmental factors account for the fluctuations. Water temperature, light availability, nutrients, salinity, carbon dioxide, water quality, composition and circulation can have a crucial role in determining the phytoplankton bloom patterns (Leterme, S. C., et al. 2008).

Higher sea surface temperatures (SST) can influence the abundance and phenology of phytoplankton organisms (van der Molen, J., & Pätsch, J., 2022). Increased SST in cold water can lead to an increase in the total number of phytoplankton and extended duration of a bloom, which was noticed before in the North Sea during warm periods (Alvarez-Fernandez, S. et al., 2012). However, when SST exceeds optimal conditions, blooming may be inhibited and abundance reduced (Desmit, X., et al. 2020). Furthermore, higher SST may promote zooplankton growth, which in turn, can lead to increased grazing and smaller chl-a biomass (van Beusekom, J. E., & Diel-Christiansen, S., 2009). In addition, different types of phytoplankton can only grow in certain temperature ranges, so rising temperatures can cause a shift in phytoplankton species (Peperzak, L., 2005).

Difference in SST can also accelerate the onset of the spring bloom and decelerate the late summer or early autumn bloom (Desmit, X., et al. 2020). This is because changes in SST can affect the stratification regime, which is important for the bloom development (Capuzzo, E., et al. 2018). As the SST rises, the density difference between the surface and bottom layers increase. This leads to stronger stratification and reduction of vertical mixing. During the spring bloom, stronger stratification will keep the phytoplankton in sufficiently illuminated upper layers near the surface triggering the spring bloom. However, if the stratification is not broken after the nutrients are depleted, it will prevent nutrient-rich deep waters from reaching the surface which can hinder the second bloom (Capuzzo, E., et al. 2018). Stratification can be broken by intense winds. The wind patterns have changed in the North Sea in the last decades. The number of days with winds exceeding 17.1 m/s decreased between March and September from 1975 to 2018 (Desmit, X., et al., 2020).

Additionally, higher temperatures and changes in nutrients can increase the possibility of the occurrence of harmful algal blooms (HAB), often called “red tides” (Quante, M., et al. 2016). HABs thrive in warmer waters (Peperzak, L., 2005). There are several species of phytoplankton capable of releasing toxins like some of the dinoflagellates (Garrison, T. S., 2012). These toxins have a negative impact on the whole food chain, causing poisoning of shellfish and fish. Those

harmful blooms can also affect humans that digest infected seafood (Santhanam, P., et al. 2019). Some of the toxins are very potent neurotoxins which can cause neurological problems and even death (NOAA 2018).

Higher temperature could also contribute to the decrease in larger phytoplankton species and increase the growth of small picoplankton (Morán, X. A. G., et al. 2010). In consequence, this could mean lower biomass. The small species of phytoplankton are prey to microzooplankton. This food chain will not contribute much to higher trophic levels (van Beusekom, J. E., & Diel-Christiansen, S., 2009). Furthermore, the increase of the small phytoplankton may have an impact on the movement of carbon to the sediments of deep ocean because the speed of phytoplankton sinking relies upon its size (Morán, X. A. G., et al. 2010).

The general pattern of the North Sea SST shows an increase. The temperature increases were 3 to even 4 times higher than the global rise in SST (Høyer, J.L., 2016). From the early 1970s to mid-2010s the SST increased by 1.6^{o}C (Desmit, X., et al., 2020). However, in the late 1970s lower-than-normal temperatures occurred in the North Sea which had affected the bloom patterns (Alvarez-Fernandez, S. et al., 2012). During those years, the blooms had been smaller than usual and started later in the year (Alvarez-Fernandez, S. et al., 2012).

Salinity can also potentially influence the plankton dynamics (Leterme, S. C., et al., 2008, Alvarez-Fernandez, S. et al., 2012), especially the maximum value of the chl-a concentration that is nutrient limited (Desmit, X., et al., 2015). In general, the salinity of the North Sea has been reported to exhibit an increasing trend from the 1960s to the early 2000s, due to the higher input of Atlantic waters (Wiltshire, K. H., & Manly, B. F., 2004, Leterme, S. C., et al., 2008). The inflow of the Atlantic water depends on the North Atlantic Oscillation Index (NAO) (Winther, N. G., et al., 2006), the difference in sea level pressure between Portugal and Iceland that can generate the westerly winds. The pattern of NAO index is difficult to predict. It has a high interannual and interdecadal variability which affects the winds, precipitation, salinity, and SST of the North Sea (Leterme, S. C., et al., 2008, Quante, M., et al., 2016). During the positive NAO, which is characterized by south-westerly winds, there is a higher inflow of warmer and more saline waters, while negative NAO that is associated with south-easterly winds reduces the Atlantic inflow to the North Sea (van Beusekom, J. E., & Diel-Christiansen, S, 2009).

The inflow of Atlantic waters is related to water mixing and it brings nutrients to the North Sea (van Beusekom, J. E., & Diel-Christiansen, S, 2009, Desmit, X., et al., 2015). Alternatively, in the coastal areas, mainly riverine discharge handles nutrients replenishment (van der Molen, J., & Pätsch, J., 2022). Higher precipitation is projected during this century (Peperzak, L., 2005), which would lead to increasing the freshwater input lowering the salinity. Consequently, it may bring larger amounts of nutrient-rich water into the North Sea. Therefore, salinity could be used as a proxy for nutrients concentration. In this case, low salinity in coastal regions may explain a higher magnitude of chl-a values (Desmit, X., et al., 2015) while higher chl-a maximums, in the northern regions, may be explained by higher salinity (Leterme, S. C., et al., 2008). However, in estuaries, larger riverine discharge may increase turbidity and decrease the light availability. Additionally, higher input of freshwater can also influence the water stratification by forming the halocline further away from the coast. Nowadays the Rhine River can lead to stratification in water column sometimes as far as 40km from the coast (Peperzak, L., 2005).

The wind strength has decreased in recent decades (Desmit, X., et al., 2020), but an increase in wave heights has been noticed in the North Sea that can influence sediment resuspension (Wilson, R. J., & Heath, M. R., 2019). According to the newest studies, the transparency of the North Sea has declined, as the water turbidity and suspended matter increased, in the last century (Opdal, A. F. et al., 2019, Wilson, R. J., & Heath, M. R., 2019). Higher concentration of dissolved organic carbon has been found in the lakes and rivers that flow into the North Sea (Opdal, A. F. et al., 2019). This change will affect the amount of underwater light and could hinder the blooms, especially in the southern part of the North Sea where light availability is considered to be the limiting factor (McQuatters-Gollop, et al. 2007) and can cause the delay in phytoplankton blooms onset (Opdal, A. F. et al., 2019).

The current trends taking place in the North Sea can have a significant impact on phytoplankton blooms. Shifts in phytoplankton bloom patterns, composition and abundance can have profound consequences. If a shift in the dynamic of those species occurs, it can impact other maritime life (Brody, S. R., et al. 2013). Zooplankton grazing is strongly dependent on bloom patterns and the kinds of phytoplankton present. Any changes in the zooplankton can have influence on well-established, in the North Sea region, fishing industry, and in consequence it can also affect human food supply. Phytoplankton play a significant role in removing carbon dioxide from the atmosphere, any change in the bloom's productivity may influence climate change. As

phytoplankton is the base of marine life, monitoring changes in their blooms are especially important.

3. Methods

3.1 Study Area Description

The North Sea was formed during Holocene flooding (Ducrotoy, J. P. et al., 2000). It is a rather shallow, epi-continental shelf sea (Flemming, N. C. et al., 2017). It lies on the Northwest European shelf, between seven countries: Great Britain (England and Scotland), France (Hauts-de-France region), Belgium, The Netherlands, Germany, Denmark, and Norway. It connects with the Atlantic Ocean through the Norwegian Sea in the north and the narrow Dover Strait and English Channel in the southwest, which is among the busiest maritime regions in the world (Quante, M., et al. 2016). In the east it borders with the low salinity Baltic Sea through the Kattegat and Skagerrak straits.

The North Sea covers an area of approximately 575 300km^2, excluding the straits (Otto, L. et al., 1990). The average depth is around 90m (Ducrotoy, J. P. et al., 2000). More than two-thirds of the North Sea basin have a depth less than 100m (Winther, N. G., et al., 2006, Opdal, A. F. et al., 2019). The shallowest bathymetry is in the south, with less than 40m depth approximately (Flemming, N. C. et al., 2017). It deepens in the north direction, with the deepest point of roughly 700m located in the Norwegian Trench (Ducrotoy, J. P. et al., 2000). In the southern part of the North Sea, several sea banks can be found with the largest one being the Dogger Bank, where primary production can be present almost the entire year (Ducrotoy, J. P. et al., 2000).

The topography of the North Sea influences the currents (Winther, N. G., et al., 2006). The circulation is anticlockwise due to Coriolis force. The water from the north drifts to the western coast as the Fair Isle Current and later splits up into Scottish Coastal Water and Dooley Current. Water that enters through the channel flows as a Continental Coastal Current next to the coasts of Belgium, the Netherlands and up to Denmark, where it mixes with Baltic waters (Ducrotoy, J. P. et al., 2000). The topography also affects the mixing of the water column (Alvarez-Fernandez, S. et al., 2012). The deeper, colder northern waters remain stratified during the summer months, with the thermocline at the depth of approximately 50m (Ducrotoy, J. P. et al., 2000) while shallow southern waters can become well mixed also during warmer months (Alvarez-Fernandez, S. et al., 2012).

Moreover, the North Sea is influenced by tides that control hydrodynamic movements (Flemming, N. C. et al., 2017). The anticlockwise rotation is present around three tidal nodes: between the Netherlands and United Kingdom, west of Denmark and south of Norway (Otto, L. et al., 1990). The tidal currents are responsible for the horizontal and vertical water mixing that disturb the stratification of the water column in the shallow southern North Sea (Quante, M., et al. 2016) and impact the vertical migration of plankton (Otto, L. et al., 1990).

The climate of the North Sea is influenced by the proximity of the continent. However, the wide connection with the Atlantic Ocean allows for the transfer of heat, matter, and momentum (Quante, M., et al. 2016). It can bring brief changes in the continent-dominated climate, as well as more long-term effects of the oceanic climate (Ducrotoy, J. P. et al., 2000). The salinity and temperature of the North Sea depend on NAO, but the hydrologic characteristics are also under continental influence (van Beusekom, J. E., & Diel-Christiansen, S, 2009) especially in the south and the east. As a consequence, salinity and SST experience spatial, annual and interannual variability (Ducrotoy, J. P. et al., 2000). In the northern part of the North Sea, the salinity reaches approximately 35 psu, while the salinity in Danish straits is lower and goes up to only 32 psu (Høyer, J. L., 2016). The SST of the North Sea is warmer to the south in summer and warmer to the west in winter.

The North Sea has an input of low saline and freshwater from the Baltic Sea, the melt waters of Scandinavia and other river runoff, especially the Rhine River. The catchment area of the North Sea is 840 000km^2 (Ducrotoy, J. P. et al., 2000). Input of freshwater is estimated to be between 295 and 355 km^3 with melting water contributing about one-third (Quante, M., et al. 2016). The biggest rivers that flow into the North Sea are the Forth, Humber, Thames, Seine, Meuse, Scheldt, Rhine, Ems, Weser, Elbe, and Glomma. The influx of river waters has a significant impact on the optical properties of the North Sea. In the south, higher riverine input and the resuspension of the sediments (Opdal, A. F. et al., 2019) is responsible for lowering the visibility and light penetration due to larger concentration of the suspended matter (Otto, L. et al., 1990). Approximately 50% of the Atlantic water that infiltrates the North Sea is later mixed with the freshwaters before moving up north into the Arctic in the form of Norwegian Coastal Current (Winther, N. G., et al., 2006).

The North Sea basin has a high population density with approximately 250 inhabitants per km^2 with the Netherlands and Belgium leading (Eurostat 2009). The countries adjacent to the North

Sea are highly developed and industrialized. Large cities like London, Hamburg, Amsterdam, and Oslo are located in the region of the North Sea. Due to the developed coastal industries such as the chemical industry, metal processing, oil refineries and shipbuilding, as well as large areas of livestock and farming production (Quante, M., et al. 2016, Capuzzo, E., et al., 2018), a significant amount of waste is being generated. As a result, pollutants, including nutrients are transported to seawater via rivers and the atmosphere (Ducrotoy, J. P. et al., 2000). The Rhine, Humber, Seine, and Elbe are responsible for bringing 56% of nitrogen and 63% of phosphorus to the North Sea (Ducrotoy, J. P. et al., 2000).

An international symposium was held in Helgoland in the late 1960s that urged a decrease in the pollution of the North Sea. In the following decades, further initiatives were taken and countries around the North Sea acknowledged the need to decrease the eutrophication (Desmit, X., et al., 2020). Measures to reduce the amount of nutrients resulted in a reduction of phosphorus input and a slightly smaller reduction in nitrogen (Desmit, X., et al., 2020). The economy of north-western Europe relies heavily on the North Sea, which is an important area of oil and gas production. It also has some of the busiest sea traffic in the world (Quante, M., et al. 2016). The North Sea has rich fisheries, and more than a million tons of fish and shellfish are caught there each year (Quante, M., et al. 2016).

Looking at the median chl-a distribution and taking into consideration differences in characteristics of the North Sea, it was decided to divide it into 6 study areas: Northwest (at the east coast of Scotland and England – region A), Central (North Sea open waters – region B), Northeast (Norwegian Trench and Skagerrak strait – region C), Dogger Bank (region D), South (between coast of England, The Netherlands, Belgium and France till the English Channel – region E) and Central east (between coast of Denmark, Germany and the Netherlands – region F)(Figure 1).

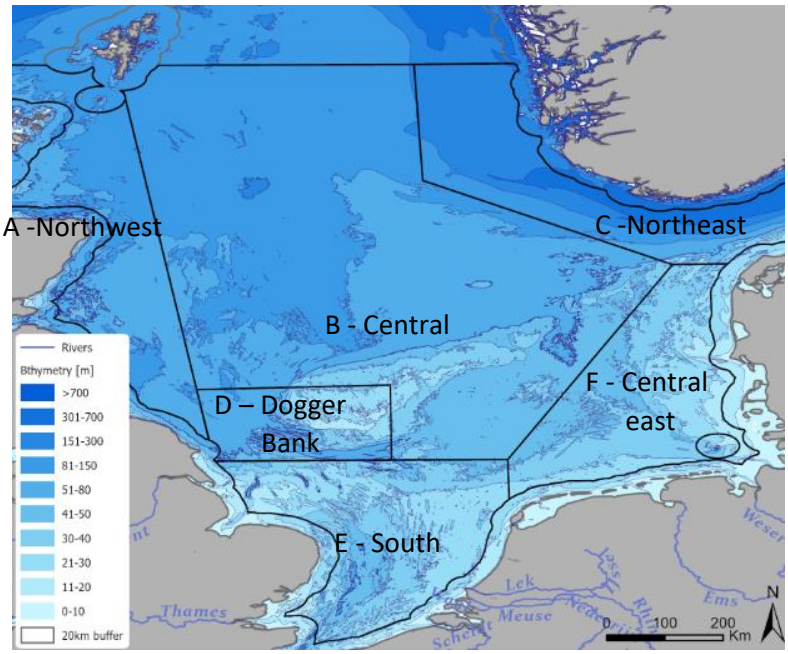

Figure 1. Study area

3.2 Environmental Variables

3.2.1 Chlorophyll-a data

The analysis was performed using satellite derived chl-a concentration data for the region of the North Sea [60-50°N, -3-10°E] covering the years 1998-2020, excluding the year 2017, as the data was unavailable. The data was extracted from the GlobColour project database (https://hermes.acri.fr)

The GlobColour project was launched in 2005. It was originally founded by the European Space Agency. It was developed to supply continuous merged level-3 ocean colour products. It supports two spatial coverages: the global Earth and extended European area. The chl-a concentration data used in this thesis was extracted from the European domain at a spatial resolution of 1/96° (i.e., approximately 1.16 km) and a temporal resolution of 8 days. It was decided to use the merged level-3 products of several satellite's sensors to provide higher coverage and to decrease the number of no data values caused by the limitation of single sensor data. Additionally, usage of a merged dataset is recommended to estimate the inter-annual variability of chl-a (Gohin, F., et al. 2020). The merged dataset employed in this study used four sensors (Table 1). The products from the SeaWiFS sensor level-2 data have a spatial

resolution of approximately 4km for the Global Area Coverage (GAC). The data from this sensor was down-scaled by using the oversampling method to achieve a finer, 1km resolution for the product of European' domain. The algorithm used to extract chl-a concentration was based on O'Reily et al., 2000. Following algorithms that had been used: for SeaWiFS OC4v5, for MERIS OC4Me, for MODIS and VIIRS OC3v5.

Table1. Sensor resolution and its time of service. Sea-viewing Wide Field-of-view Sensor (SeaWiFS), Medium Resolution Imaging Spectrometer (MERIS), Moderate Resolution Imaging Spectrometer (MODIS AQUA), Visible Infrared Imaging Radiometer Suite (VIIRS).

Sensor	**Resolution**	**Start Date**	**End Date**
SeaWiFS	GAC 4 km	1997-09-04	2010-12-11
MERIS	1 km	2002-04-28	2012-04-08
MODIS AQUA	1 km	2002-07-03	Present
VIIRS	1 km	2012-01-02	Present

The binning schema to create the merged data from these 4 sensors, consisted of 5 steps. Firstly, level-2 data for each sensor was transformed to the European Integerised SINusoidal projection (ISIN) grid providing the spatial binned level-3 data of chl-a concertation for each sensor. Then, the data was binned into daily products. The daily product for each of the sensors was merged into one dataset. The merged products chosen for this study were generated by the Garvel-Sigel-Maritorena (GMS) model (Maritorena and Siegel, 2005). This model is based on the normalised water-leaving radiance $L_{wN}(\lambda)$ (Maritorena and Siegel, 2005). When the pixel had multiple values of normalised leaving radiance available, the data from different sensors was combined and then used to produce the merged dataset. If the bands of the sensors were different, the better spectral resolution is used (IOCCG, 2007). After merging the dataset, the daily chl-a concentration data was binned into 8-day products. Finally, it was transformed into mapped products in the Plate Carrée projection.

The downloaded data was stored in the Network Common Data Form version 4 (netCDF-4). Every pixel in the main netCDF file contained two variables. The sub dataset used in this study was the 8-day chl-a concertation mean and 8-day chl-a concertation error rate (Table 2). The data was extracted for the Case 1 waters (CHL1). Case 1 waters are waters that have their optical properties dominated mainly by the phytoplankton and CDOM that is released by it, while Case 2 waters have their optical properties primarily influenced by other inorganic mineral particles

and microbubbles (Mobley, C. D. et al, 2004). Case 1 waters can be found mostly in open waters, while Case 2 waters are present mainly in coastal areas (GlobColour Product User Guide, 2020), which were excluded from this analysis.

Recent studies show that the North Sea has experienced a decrease in water clarity. However, the non-algal suspended matter is present mostly in the shallow south and south-eastern parts of the sea (Wilson, R. J., & Heath, M. R. 2019). It was still decided to use data for Case 1 waters even in the south and south-east regions due to several reasons. Firstly, the classification of water bodies into Case 1 or Case 2 waters is problematic as the transition between them cannot be clearly distinguished (Mobley, C. D. et al, 2004). Secondly, the optical characteristics for Case 2 waters can differ significantly between the water bodies (Darecki, M., Weeks, A. et al, 2003). Using a single algorithm for those types waters is not appropriate, and the data can still be incorrect (Darecki, M., Weeks, A. et al, 2003). Due to the difficulty of creating algorithms that will take into consideration all the factors of specific water bodies and derive the chl-a data for Case 2 waters locally, this data is not easily accessible. It was only available in the GlobColour database until the year 2012, meaning that the time series would be much shorter, and the observation of any trends would be more difficult.

Table 2: Sub dataset of 8-d chlorophyl-a concertation used during the analysis: mass concentration of chlorophyll-a [mg/m^3] in sea water (CHL1 mean) and error rate (CHL1 error)

Name	**Image file type**	**Unit**
CHL1 mean	32-bit floating-point	mg m-3
CHL1 error	16-bit integer	%

3.2.2 Sea Surface Temperature data

The SST data was downloaded for the same region and period. The data used was extracted from the OceanColor database (https://oceancolor.gsfc.nasa.gov/). It was derived from the MODIS-Terra satellite. The downloaded data was a mapped product in Plate Carrée projection with monthly temporal resolution and spatial resolution of 4km x 4km. The file type was 16-bit integer with a scale factor of approximately 0.005. It was in NetCDF 4 data format.

3.2.3 Seas Surface Salinity data

Monthly means of Sea Surface Salinity data were downloaded from Copernicus Marine Service (https://resources.marine.copernicus.eu) for the North West-European Shelf. Salinity product used in this study was generated using a coupled physical-biogeochemistry model. The spatial resolution was 7km x 7km. The data takes into consideration only 1m of thickness when the depth of the North Sea is higher than 50m and less than 1m where the bathymetry is lower than 50m. The data was in NetCDF 4 format.

3.3 Data analysis

3.3.1 Chlorophyll-a time series analysis

The chl-a data is available between the 5^{th} and 6^{th} week of the year (beginning of February) until approximately the $44^{th}/45^{th}$ week of the year (beginning of October) in the north part of the North Sea and between the $4^{th}/5^{th}$ and $45^{th}/46^{th}$ week of the year in the south of the North Sea. The winter months are missing from the data due to low light availability in the winter. The limiting factor for the blooms in North Sea is solar radiation. Therefore, no blooms should be present at that time, with possible exception of the Dogger Bank region (Ducrotoy, J. P. et al., 2000). The data between the years 1998 to 2001 was excluded from the analysis due to too many missing values. The reason for this is that during this period the data was derived only from the SeaWiFS sensor. From 2002 the MERIS sensor became active, and the merging of those datasets allowed for better coverage. In the end, only the time series between 2002 and 2020 was analysed with exception of the year 2017 as this data was missing from the GlobColour database.

The netCDF data consisted of an 8-day chl-a mean value and corresponding scaled error estimation. Firstly, the variables were extracted from netCDF files and saved in separate GeoTIFF format. The WGS84 coordinate system was assigned to each of the chl-a mean and error estimation files. To understand the data better, and to flag regions with high errors, the error estimation files were recalculated into weights. To do that, the error estimation files were divided by 100 to get values in decimal instead of percentage. Then the resulting values were subtracted from 1 to get a weights file that consisted of values from 0.001 to 1, where the lowest values meant that the pixel had the highest errors. All calculations were done using

gdal_translate program and gdal_calc.py which belongs to GDAL library. The median of the weight error files, and chl-a median was computed for the whole time series using ArcGIS Cell Statistics for batch files. This was done to get the general view of the data, understand the error propagation and to decide on the sub-areas that will be used in TIMESAT software to investigate the phytoplankton phenology parameters (Figure 2).

Larger errors were present in regions of low chl-a concentration, reaching high values near the Norwegian trench (Figure 2A). However, the largest errors were near the coast. This may be due to the large image resolution of 1km x 1km. It could cause pixels to be incorrectly classified as water instead of land. Secondly, river inflow leads to higher turbidity in coastal areas and a higher concentration of suspended particulate matter. The time series of chl-a and error estimation files were clipped per each of the study areas. A buffer of 20 km from the coast was created, and those pixels were excluded from the analysis.

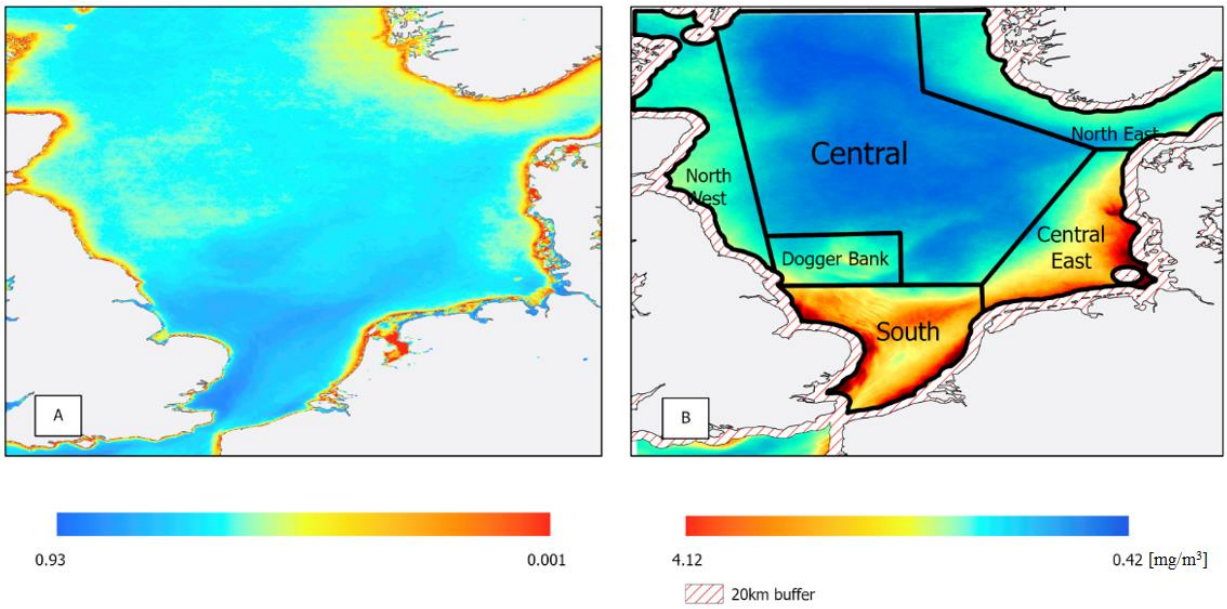

Figure 2. A. Weights of error estimation [unitless] - value of 1 indicate pixels with no errors, value of 0.001 indicate pixels with the highest error (mostly located in the coastal zones). B. Mean of chl-a concentration [mg/m^3] for the whole time series from 8-day binned chl-a values with 20km buffer from the land – red dash lines. The highest chl-a concentration is found in region E (South) and F (Central-East) and the lowest in region B (Central).

3.3.2 Phytoplankton phenology parameters in TIMESAT software

TIMESAT was developed at Lund University for the study of vegetation index time-series, extracted from satellites (Jönsson, P. & Eklundh, L., 2017), but it can manage other types of remotely sensed data (Jönsson, P. & Eklundh, L., 2017). It was already used to, for example, analyse meteorological index, fire data (Jönsson, P. & Eklundh, L., 2017), seasonal freeze-thaw cycle in Arctic lakes (Šmejkalová, T., et al. 2016) and sea surface chlorophyll-a data (Benzouaï, S., et al. 2020).

One of the reasons the decision was made in favour of using TIMESAT is that it is an open-source software and therefore easily available. Secondly, there are various build-in time series smoothing methods and the user can experiment and change settings to find out what works best for their data. Finally, it has already been tested for uses other than those originally intended, with consistent results (Benzouaï, S., et al. 2020). There are other alternatives to TIMESAT such us building a model and programming an algorithm to smooth the chl-a data, that may provide lower-uncertainty results. Such methods require an extensive knowledge of programming languages and a need to verify the created algorithm, for example by checking the in-situ data. Concluding that is why TIMESAT software, version 3.3 was used to analyse the phytoplankton phenology parameters. TIMESAT was run using MATLAB R2020a.

TIMESAT allows the calculation of seasonality parameters as illustrated in Figure 3. However, in this thesis only 5 parameters were under investigation: start of the phytoplankton bloom SOB (a), end of the phytoplankton bloom EOB (b), length of the phytoplankton bloom LOB (c), peak time of the phytoplankton bloom PTB (e)– the time when chl-a reached the maximum value, and peak value of the phytoplankton bloom PVB (f) – the maximum value of chl-a biomass. TIMESAT can process sequential data in ASCII file and image data in binary format. The latter choice was used during this analysis.

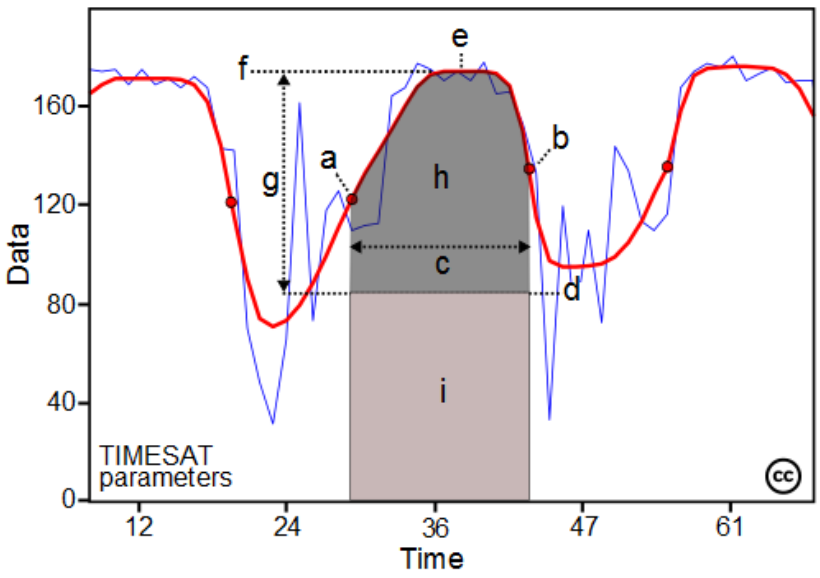

Figure 3. Seasonality parameters generated in TIMESAT: (a) beginning of season, (b) end of season, (c) length of season, (d) base value, (e) time of middle of season, (f) maximum value, (g) amplitude, (h) small integrated value, (h+i) large integrated value.
Source: Eklundh, L., & Jönsson, P. (2017). TIMESAT 3.3 with seasonal trend decomposition and parallel processing Software Manual

To obtain the data that can be handled by TIMESAT, the GeoTIFF format was translated into ENVI image format with the accompanying ASCII header files. To start analysing the time series in TIMESAT, a text file containing the list with the paths to the chl-a files of specific area needed to be created. To do that, a windows command prompt was used, and 6 different lists, one for each region, were generated. Those file lists were later uploaded into the TSM_GUI program, which is used within TIMESAT to analyse the time series. It allows us to investigate and find the best fit for smoothing the raw data function, interpolate the missing values, check the quality, and reduce the noise present in the raw data. However, before the lists of files could be uploaded into TSM_GUI, they were modified. To be able to handle the text file containing the list of filenames, TIMESAT needs a header, in that file, with the number of files that the list contains. Furthermore, TIMESAT can only derive the seasonality parameters for the n-1 seasons; therefore, a dummy year was created in the file list and the number of extra files were added in the header.

Inside TSM_GUI program a setting file is created for the selected image pixels. This file holds all the specification and methods used in analysing the time series. To create the setting files, the data was first investigated for different random pixels in each of the regions. After investigation of the data, it was determined that in most of the study area there is more than one

peak present in the phytoplankton bloom over one year (called later S1 for spring bloom and S2 for late summer, early autumn bloom), which agrees with the findings of earlier research (McQuatters-Gollop, A., et al. 2007, Quante, M., et al. 2016).

In TIMESAT, three different methods are available to find the best function fit to smooth and reduce the noise from the raw data and to fill the gaps that can be present in the timeseries due to, for example: presence of clouds, sun glint etc.: Savitzky-Golay filtering, least-squares fit to asymmetric Gaussian function and double logistic model function (Jönsson, P. & Eklundh, L., 2017). Those methods are based on temporal interpolation, which is better suited for the phenology studies where the spatial differences can be large (Moreno, Á., et. al, 2014). They can be applied to any dataset in which the measurement points are occurring one after another at even intervals. Savitzky-Golay is a local filtering method, meaning it does not assume shape and magnitude of phenological data (Moreno, Á., et. al, 2014). These methods are better in picking fast changes during the growing season (Cai, Z., 2017). Savitzky-Golay filtering method (S-G method) replaces the raw data values by the linear combination of nearby values in the specified filtering window (Jönsson, P. & Eklundh, L., 2017). It is a weighted average in which the weights are decided by fitting a least-squares fit polynomial function to the neighbouring points. Double logistic and asymmetric Gaussian are global filtering methods. They fit the data into mathematical functions (Cai, Z., 2017) and because of that can be less flexible to high interannual changes (Moreno, Á., et. al, 2014).

An experimental approach was performed to check which method was the most suitable to smooth the weighted chl-a data. The last two methods showed an overestimation of the values by creating large peaks where no data was present (Figure 4); therefore, the S-G method was chosen instead. It had the best fit to the original data and allowed more details to be kept. However, it also displayed a behaviour of creating artificial peaks and overestimating the length of the S2 blooms in situations where no data was present (Figure 5). Those values were later discarded from the study.

An important parameter in the S-G method is the window size that indicates how many neighbouring points will be used for the filtering. The larger the value of the window size, the higher degree of smoothing would be applied. In this case, a window size of 3 was chosen as it gave a good fit and smoothed out the noise that was present in the data without losing too many of the details. Since each data point represents a mean value from 8 days, smoothing performed

over three consecutive points encompasses a period of 24 days. It is also better to use an odd value for the smoothing window size, because then the new smoothed value is in the same position (same date) as the original value. The S-G method can be expressed by the formula:

$$Y_j * = \sum_{i=-m}^{i=m} \frac{c_i y_{i+j}}{N}$$

(Equation 1)

where Y^* is the resultant chl-a value, y is the original chl-a value and c_i is the convolution coefficient that can be found in tables for the specific window size and polynomial order, N is number of convoluting integers, and m is half width of the smoothing window.

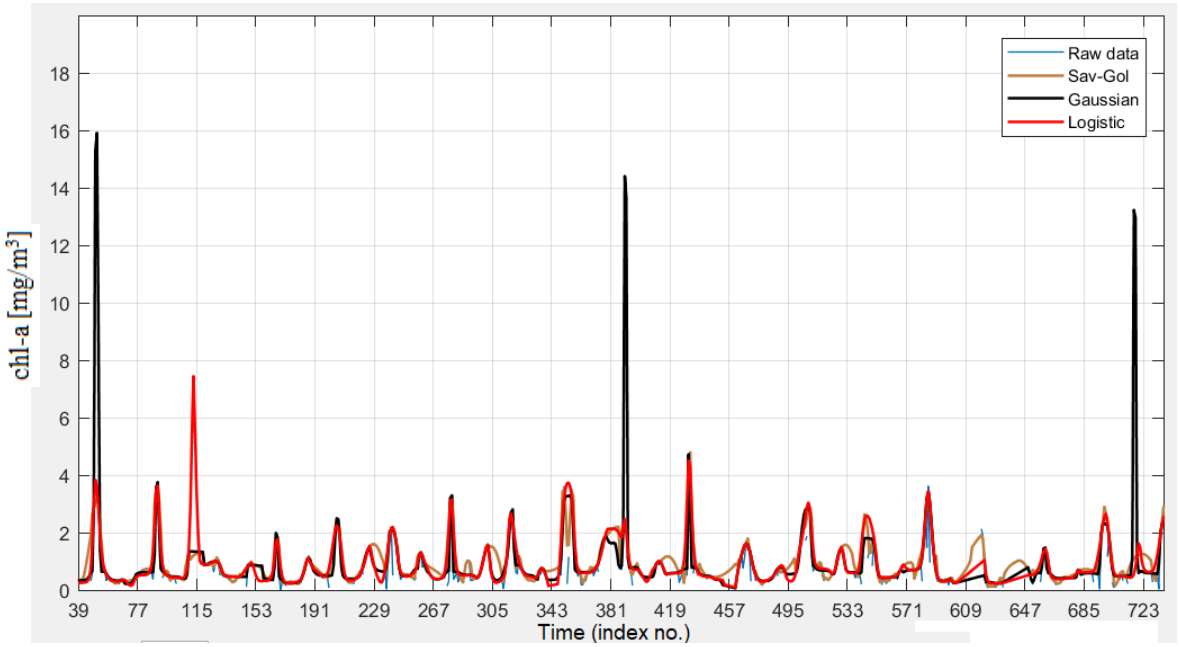

Figure 4. Example of the overestimation of chl-a [mg/m^3] values between time index 39-76, 381-418, 685-722 asymmetric gaussian function and between 77-114 the double logistics function. Savitzky-Golay (yellow line), Asymmetric Gaussian (black line), Double logistics (red line).

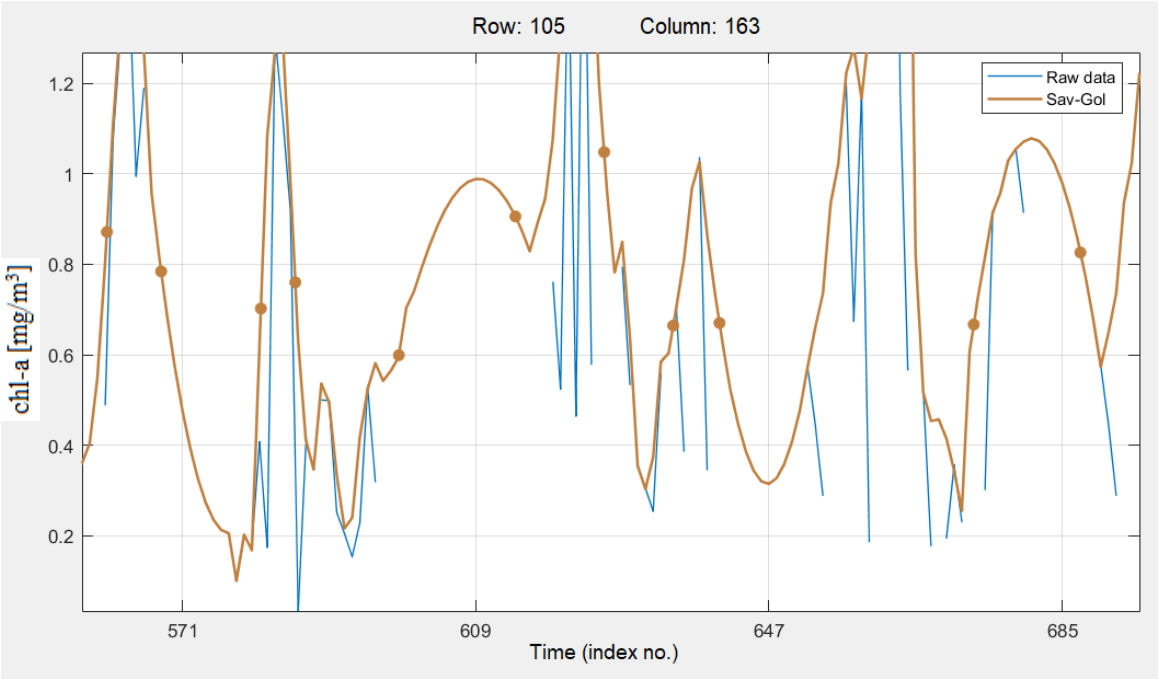

Figure 5. Example of artificial peak (around index no 609) created by Savitzky-Golay function (yellow line).

To accommodate for the negatively biased noise, which is caused by for example clouds, ozone, dust, or aerosols present in the atmosphere (Moreno, Á., et al. 2014) and to improve the results of the S-G fitting method, the number of envelope iteration was set to 3. This means that the fitting line was generated 3 times and each time the points that were below the previous fit line got a lower weight and became less significant. The adaptation strength was applied to the envelope iteration. This value shows how strong the upper envelop iteration will be. The higher the value the stronger the adaptation. The usual value is between 2 and 3 (Jönsson, P. & Eklundh, L., 2017) in this case an adaptation strength of 3 was chosen as it allowed for the best fit of the filtering function to the raw data.

Before it is possible to derive any parameters in TIMESAT, it is important to choose a method for defining the start and the end of the growing season. In this case the biomass threshold method was chosen, which is one of the methods used in phytoplankton phenology studies (Brody, S. R., et al. 2013). It was first used by *Siegel et al*. in 2002 and has since been used many times in studies of phytoplankton blooms (Brody, S. R., et al. 2013). This method is also in line with the methodology used by Benzouaï, S., et al, 2020 that used the TIMESAT software for their phytoplankton bloom analysis in the Algerian Sea. The biomass threshold method indicates the start and end of the bloom when chl-a biomass rises 5% above the median value (Siegel at al. 2002).

The bloom initiation values were computed for each region using the median chl-a data. Due to TIMESAT limitations, only one threshold initiation value can be used for the whole region. Following the methodology of Benzouaï, S., et al. 2020 the median chl-a data distribution was used. To remove the influence of the outliers, the calculated median values per region for the whole time series were first cleaned out by removing the values above the upper and below the lower fence (Equation2). It was done using MATLAB 2020a software (Figure 6).

$$\text{Lower fence} = Q1 - 1.5\,(IQR)$$

$$\text{Upper fence} = Q3 + 1.5\,(IQR)$$

$$IQR = Q3 - Q1$$

(Equation 2)

where Q1 is the first quantile, Q3 the third quartile, and IQR is the interquartile range.

The final initiation values were computed by adding 5% to the calculated median values.

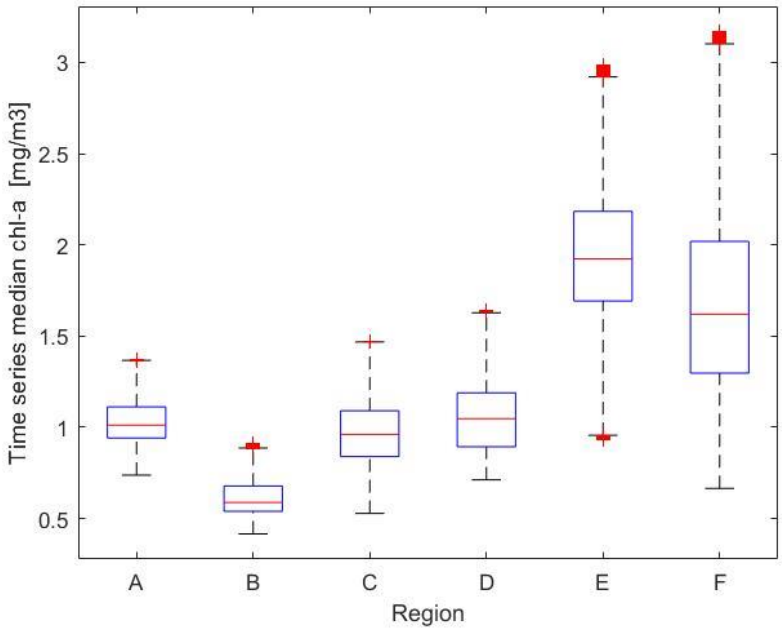

Figure 6. Time series median chl-a [mg/m^3] values and interquartile range per region after outliers' removal.

In TIMESAT, different methods are available for finding the beginning and end of the growing season. The absolute value, relative amplitude and STL trend were not suitable for the chl-a data in the North Sea. It was decided to use the seasonal amplitude method instead. In the seasonal amplitude method, the user decides a threshold between 0 and 1. The threshold is computed between the base value which is the average of minimum value from the left and right side of the function peak and the maximum value of that peak (Figure 3). When the function reaches the threshold, TIMESAT identifies it as the start/end of the growing season. Therefore, the position of the initiation value in the data distribution for each of the region, was computed and used as the threshold value in TIMESAT.

After all settings were decided, the setting file for each of the regions was created (See Appendix). The saved setting files for each region were imported one by one into the TSF_process tool in TIMESAT to extract the phenological parameters. Later, the TIMESAT TSF_sea2img tool was used to generate phenological parameters maps of the SOB, PTB, PVB, LOB and EOB, for each year and region. The result files created for each parameter consisted of separate files for each of the blooms seasons (S1, S2), as well as the data for both blooms together. For further analysis only the S1 and S2 parameters files were used.

The output files had to have their extension changed to .img to allow other software to read it. Additionally, for each of the resulting files a header was created using a python script. The resulting files were later modified using the gdal_calc.py program. Firstly, the values representing no data were converted to an actual no data mask. Secondly, the SOB, EOB and PTB had their output values displayed in the time index. Due to having 35 files (33 in the northeast region and 37 in the south region) per year the first year (2002) had values from 1 to 35 (33, 37), second year (2003) had time index from 36 (34, 38) to 70 (66, 74) and so on. Gdal_calc.py was used to change that display to the day of the year instead. This was done by subtracting the specific number from the raster image. For example, SOB, EOB and PTB raster for the year 2003 had the value of 35 (33, 37) subtracted from it, year 2004, had a value of 70 (66.74) subtracted and so on. That way the resulting value indicated which file number it referred to. The file number was later adapted and displayed as the day of the year. Finally, the raster files were inspected for inconsistencies in ArcGIS Pro.

Some pixels displayed uncertain values, which were further inspected. The uncertain values were related to the peaks that S-G filtering method created when no data was present. This situation happened because of the incomplete dataset for the region as the satellite imagery is

not available during the winter months when not enough light reaches the North Sea. In those situations, TIMESAT created artificial peaks or joined the S2 peak of the previous year to the S1 peak of following year resulting in incorrectly interpreted bloom season. Upon more in-depth investigation of these cases, the conclusion was reached that the chl-a concentration is still high from the time the data is available (beginning of February) and it just starts to decrease. This means that the bloom reached its peak somewhere between October and February, when the satellite imagery data is not available (Figure 7).

This situation was visible in most of region C, the middle east of region B, parts of the east of region D and west of the region E (Figure 8). Additionally, in region D the bloom patterns were too complex. TIMESAT can analyse one or two annual seasons but in Dogger Bank many of the pixels had 3 bloom seasons picked up. Those peaks in region C, B, D and E were discarded from all raster files. This was done by assigning no data values for all the pixels that had values lower than 0 for the SOB (those values would indicate SOB started in the previous year) and values higher than 35 (33, 37) for the EOB (those values would indicate that the bloom finished the following year). To clear the rest of the parameters (PTB, PVB, LOB) of the incorrectly calculated values, the same pixels had no data values assigned to them. The number of correct pixels values was counted in percentage to see which region is the most dependable (Table 3). After the investigation, it was decided to discard S2 from the analysis due to too many missing values.

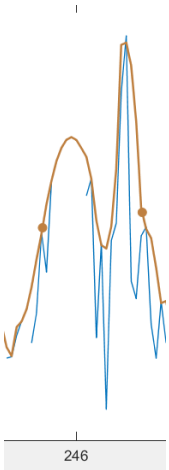

Figure 7. Example of a peak that is not correctly recognized by TIMESAT due to missing data during winter months in a pixel located in the central part of region B

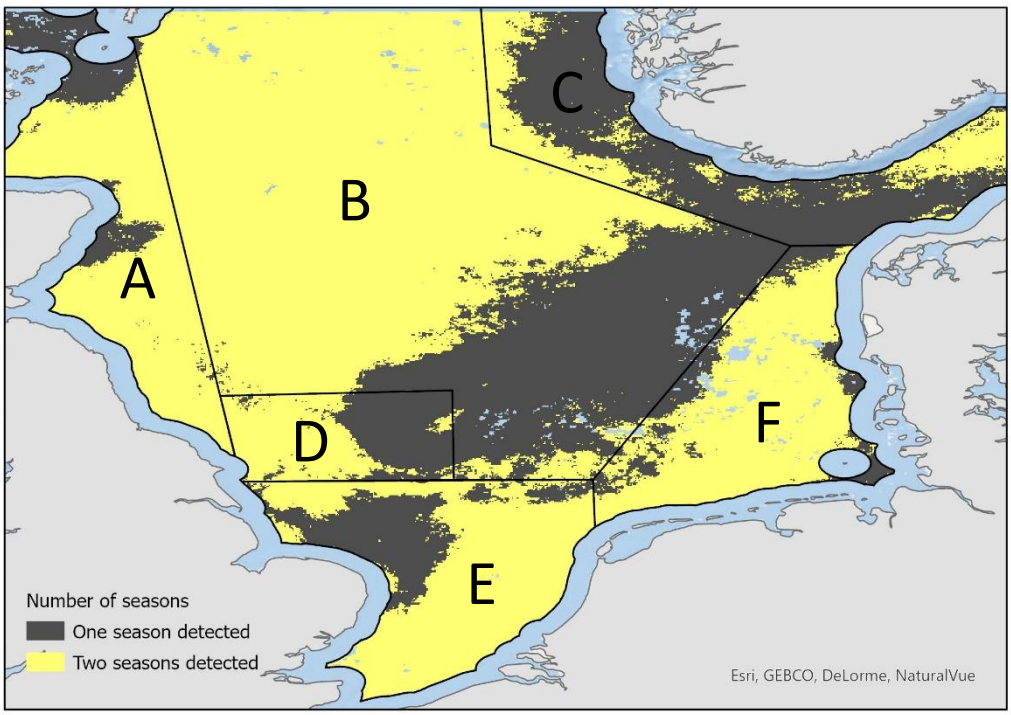

Figure 8. Number of seasons detected by TIMESAT

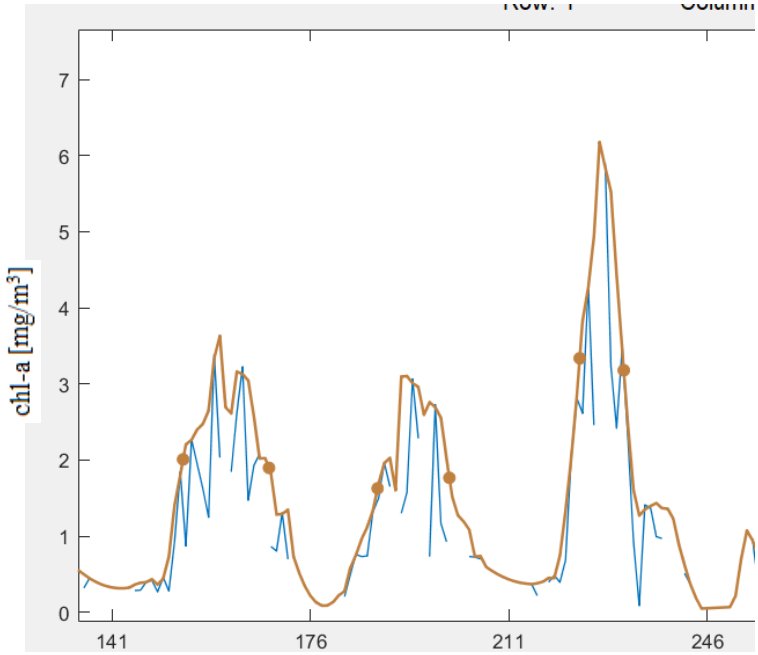

Figure 9. Example of northwest pixel of region A that has correctly detected only one season

Table 3. Number of correct pixels values per region per season in percentage.

		2002	2003	2004	2005	2006	2007	2008	2009	2010	2011	2012	2013	2014	2015	2016	2018	2019	2020
S1	A	95	95	96	97	93	94	96	93	87	90	92	95	92	95	94	92	92	86
	B	58	78	74	71	78	77	75	71	65	69	78	76	74	75	75	71	71	68
	C	29	65	41	35	48	54	24	21	41	46	25	51	45	39	31	53	58	0
	D	51	54	0	49	51	56	66	55	54	48	57	52	60	51	58	50	46	44
	E	65	54	67	76	72	75	71	84	71	55	63	68	67	62	65	79	68	69
	F	65	75	67	68	68	76	68	70	73	70	71	75	69	74	71	70	67	63
S2	A	48	51	70	58	56	43	49	54	31	48	48	57	42	45	47	40	40	43
	B	13	22	39	22	29	34	25	30	26	34	29	25	16	27	22	28	23	22
	C	7	6	11	8	15	18	6	7	10	9	4	6	6	9	10	12	10	12
	D	9	16	0	28	37	35	27	18	15	31	28	20	24	21	19	11	17	19
	E	30	18	31	33	32	32	29	20	26	19	22	27	25	23	23	23	18	16
	F	30	34	21	32	39	46	26	16	18	9	21	38	19	28	14	22	22	28

After excluding pixels with incorrect values, the mean error estimation values were calculated per year and region. This was done by summarizing 35 (33 in the northeast region and 37 in the south region) files for each pixel and then dividing sum of each pixel by the number of files for the specific region. Later, the pixels that were excluded from SOB, PTB, PTV, EOB and LOB were also discarded from the mean errors' estimation per region and year to avoid introducing bias. Finally, the weighted average was calculated for each of the parameter, getting 18 values for each of the year and region. All the calculations were done using MATLAB 2020a.

3.3.3 Analysis of Sea Surface Temperature time series

The SST data was interpolated from the original spatial resolution of 4km x 4km to match the chl-a data. It was unscaled, the raw data was scaled with the factor of 0.005 and changed into GeoTiff format. It was done using GDAL library. Later, the mean values of winter (that is December of preceding year, January, and February of that year) and summer (June, July, and August) SST were calculated for each of the region. However, data for June of 2001 needed to be interpolated before the calculation due to missing values. This was done by using the focal statistics function in ArcGIS Pro. A statistical value was calculated for each cell using a rectangle neighbourhood with the width and height of 5. Finally, the same pixels that were discarded from the parameters data due to errors, were also excluded from the SST data using gdal_calc.py. To do that, firstly, the numbers of rows and columns of seasonal SST mean raster were changed to match the bloom parameters data. After investigation of the data distribution,

it was decided to calculate median instead of mean value as a representation of SST data for summer and winter seasons for each of the regions using MATLAB R2020a.

3.3.4 Analysis of Seas Surface Salinity time series

Monthly salinity data was extracted from the netCDF file format to GeoTIFF. The spatial resolution of the salinity data was interpolated to match the chl-a data and it was clipped to specified regions. Similarly, to SST data, the seasonality of SSS time series was checked. The mean values for summer (Jun., Jul., Aug.) and winter (Dec., Jan., Feb.) were calculated. Finally, following the same methodology as in SST data preparation, the pixels that were excluded from the bloom parameters data were also discarded from the SSS data.

3.3.5 Correlation analysis

A temporal analysis was performed to see if any trends were present in the data for each individual phenological parameter, SST, and SSS. The data was also investigated for correlation. Linear regression was used to characterise relationships between phenological variables. Furthermore, it was analysed wheatear SST and SSS are factors that influence the bloom timing, length and intensity of the blooms. The potential dependencies of mean value of SST and SSS data for June, July and August of the preceding year were checked against the bloom data to see if it had any influence on the phenological parameters. The same analysis was done for winter season considering the mean value for SST and SSS data from December of preceding year till February of that year. The coefficient of determination was calculated.

3.3.6 Statistical tests

The IBM SPSS Statistic program was used to perform statistical tests to check if the differences between the parameters in the regions were statistically significant. To do that it was decided to check if the data meets the assumptions needed to perform the one-way ANOVA test (Ostertagova, E., et al, 2014).

One-way ANOVA has 6 assumptions that need to be met by the data. The first 3 assumptions of independence of observations, the independent variable having two or more categorical

independent groups, and dependent variables having interval or ratio level met. The rest of the assumptions (normal distribution of dependent variable, no significant outliers in the data and homogeneity of variance) were checked using SPSS Statistic.

The investigation of normality was performed by using the Shapiro-Wilk test. The result of the test showed that not all regions met the assumption of normality. Regions A, B and F did not indicate the rejection of the null hypothesis Ho about the normal distribution. The bloom parameters in region C, D and E, according to the Shapiro-Wilk test, showed that they were not always normally distributed. The one-way ANOVA is a robust test for the violation of the normal distribution of data and can tolerate the data that is not normal with only a small consequence of Type I error (Driscoll, W. C., 1996). Type I error occurs when the null hypothesis is rejected when it should not be discarded. Due to the robustness of one-way ANOVA, the normality of data was also investigated visually. The visual interpretation was done by checking the q-q plots and the data distribution in histograms (Figure 10). Visual interpretation of the graphs showed that region C had the least normal distributed data. What is worth mentioning is that region C (Norwegian Trench and Skagerrak strait) had the highest error present in the data (Figure 2) and many pixels needed to be discarded from the analysis. The average numbers of correct pixels per year was approximately only 39% (Table 3).

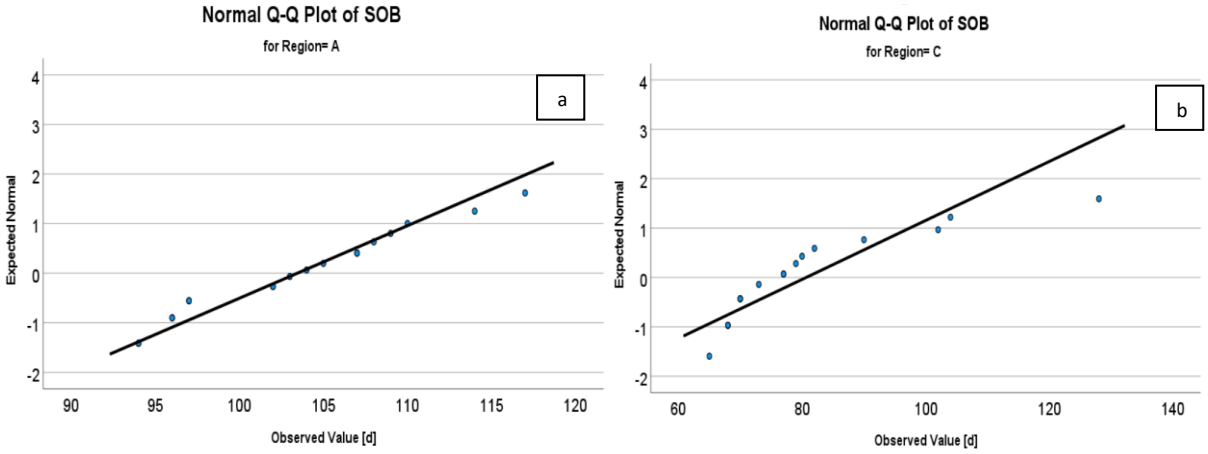

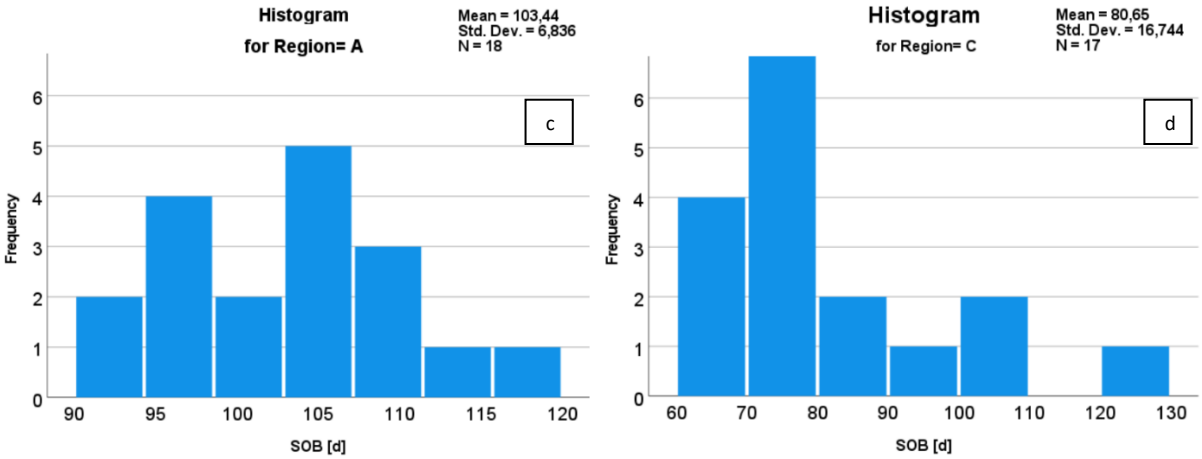

Figure 10. Example of normal distributed data for SOB [d] in region A ($p>0.05$) shown using q-q plot (a) and histogram (c) and not normally distributed data for SOB [d] in region C ($p< 0.05$) shown using q-q plot (b) and histogram (d)

Secondly, the data was investigated for outliers by checking the boxplots (Figure 11). Only region B did not show any extreme values and in the rest of the regions the outliers were present in at least one of the parameters. Finally, the Levene test was performed to investigate the assumption of homogeneity of variance. The test results showed that the variances were not homogenous.

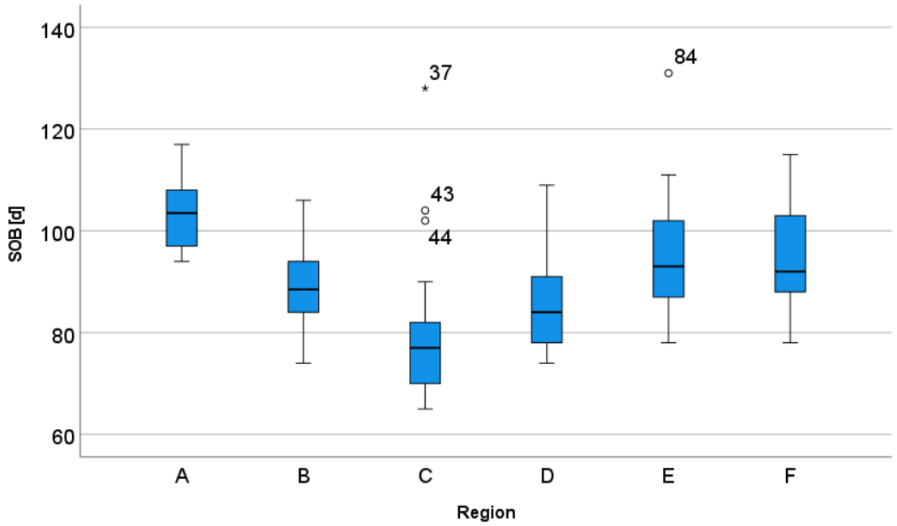

Figure 11. Example of outliers found in the data. Boxplots of SOB [d]. Region E have one outlier (No. 84 2013, 184 DOY), region C 3 outliers (No. 37 2002, 195 DOY – extreme value, No. 43 2008, 149 DOY and No. 44 2009, 144 DOY)

Due to not all data meeting the requirements of normal distribution, homogeneity of variance and the presence of outliers in the parameters. It was decided that the parametric one-way ANOVA test will be not suitable for the data. The non-parametric Kruskal-Wallis test, also

called one-way ANOVA on ranks (Ostertagova, E., et al, 2014), was conducted instead as an alternative test. The Kruskal-Wallis test ranks all the data from smallest (1) to largest (N) rank. If the same value appears in the data more than once, it is called a tied value. Tied values are given as an average of the ranks (Ostertagova, E., et al, 2014).

The Kruskal-Wallis test can be expressed by the formula:

$$H = \frac{12}{n(n+1)} \sum_{j=1}^{g} \frac{R_j^2}{n_j} - 3(n+1)$$

(Equation 3)

where n is the number of observations in all the groups, g is the number of groups, R_j is the sum of ranks in the specific group, n_j is the number of observations in each of the groups.

In SPSS, the Kruskal-Wallis test is automatically adjusted for ties that were present in the data. The correction is done using the formula:

$$H_{adj} = \frac{H}{D}$$

(Equation 4)

where D is the correction factor and is calculated by:

$$D = 1 - \frac{\sum(t_i^3 - t_i)}{(n-1)n(n+1)}$$

(Equation 5)

where t_i is the number of ties for the rank value i.

The Kruskal-Wallis test only identifies if there is a significant difference between the groups. Based on the result of the test, it was concluded that in each of the variable's distribution there is at least one region that is significantly different from the others ($p<0.01$). However, to determine between which regions the differences are statistically significant, post hoc pairwise comparisons using Dunn-Bonferroni approach were conducted.

The Dunn test is calculated by the formula:

$$Q = \frac{r_i - r_j}{\sigma_i}$$

(Equation 6)

where, r_i is the mean rank of group i and r_j is the mean rank of group j and σ_i is calculated as:

$$\sigma_i = \sqrt{n(n+1) - \frac{\sum \frac{(t_i^3 - t_i)}{n-1}}{12(\frac{1}{n_i} + \frac{1}{n_j})}}$$

(Equation 7)

where n is the total number of observations, t_i is the number of ties for the rank value of i, n_i and n_j are the number of observations for group i and group j.

The Bonferroni adjustment is done to lower the probability of making Type I errors that increases in case of multiple comparisons. The adjusted value is calculated as follows:

$$p - value = p * m$$

(Equation 8)

where p is the original p value and m is the number of comparisons made which in this case would equal 15 (6 regions were compered).

Additionally, the SPSS Statistical Software was used to test if the temporal changes in blooms' parameters, SSS and SST in winter and summer seasons show a significant increase or decrease. Furthermore, the same tests were run to check if SSS and SST have an impact on surface phytoplankton blooms. To do that, the Pearson correlation coefficient r was calculated. It was assumed that if a correlation exists between two parameters it would be linear. Pearson's r has values between -1 and 1 with -1 being a negative correlation, 1 positive correlation and values close to 0 mean no correlation. The correlation coefficient was calculated by the formula:

$$r = \frac{\sum_{i=1}^{n}(x_i - \bar{x})(y_i - \bar{y})}{\sqrt{\sum_{i=1}^{n}(x_i - \bar{x})^2 \sum_{i=1}^{n}(y_i - \bar{y})^2}}$$

(Equation 9)

where x_i and y_i are corresponding observations, $\bar{x}$ and $\bar{y}$ are the mean values and n is the number of observations.

Correlation tests were done for the data of the whole North Sea, and it was also checked per region.

4. Results

The following section will describe the findings of temporal and spatial analysis of phytoplankton spring blooms and potential impact of SST and SSS in 2 seasons, winter (Dec. of proceeding year, Jan., and Feb.), and summer of proceeding year (Jun., Jul., Aug.) on the spring phytoplankton blooms parameters for the whole the North Sea along with more in detail analysis of six specified regions.

4.1 Characteristics of spring blooms parameters and factors influencing them

There were no significant temporal changes in the time of occurrence of S1 phytoplankton bloom over the years 2002-2020 found through this analysis. According to the study spring SOB begins on average on the 91 DOY (1st of April) and ends on average on 148 DOY (28th of May) in the North Sea. The spring LOB lasts approximately 57 days with the PTB on average on 119 DOY (1st of May). The median values of the PVB showed a significant ($p<0.05$) negative temporal shift in the study area, with the Pearson correlation coefficient equal to $r=-0.54$ (Figure 12). The same trend was visible in mean values of the PVB, however it was not significant ($p>0.05$). On average the PVB reached 4.3 mg/m^3, however there is a significantly statistical difference between the PVB in the north and the PVB in the south and the central east of the North Sea with the last two reaching much higher values (Figure 15b). It is important to remember that for this analysis due to the lack of data for recent years of chl-a concentration for Case 2 waters the data for Case 1 waters was used in the south and the central east (region E and F) instead.

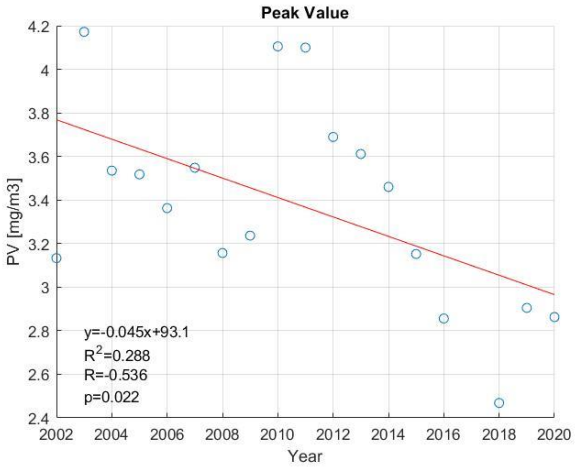

Figure 12. Decreasing trend y=-0.045x + 93.1 (red line) of median of the PVB [mg/m^3] between 2002-2020 (ex.2017) in the North Sea., correlation coefficient r=-0.536, coefficients of determination R^2=0.29, correlation significant at a 0.05 level (2-tailed) p=0.022

Further analyses were conducted to see if there are any significant correlations between the bloom parameters and to investigate if SST or SSS have a significant impact on the phytoplankton blooms. SOB, PTB and EOB, as expected, show a strong positive correlation with the correlation coefficient between r=0.89 to r=0.97 for p<0.001. The high correlation between these parameters is to be expected. If the season starts later then the peak time and the end of the bloom will likewise start later.

There are three more high correlations that were found in the data. The first correlation proves that the later the day of the end of the bloom is, the longer the bloom season will be. The correlation coefficient was approximately r=0.71 with a p<0.001 (Figure 13a). This high correlation is not surprising. Similar positive correlation was found between the day of the highest value of chl-a concentration and length of the bloom, although the value of correlation coefficient was lower than in correlation between the end of the bloom and the season length, and equalled r=0.51 with a p <0.001 (Figure 13b).

The interesting correlation was found between the PVB and the temperature in the summer season. It indicates that the higher the temperature in the summer season, i.e., from June to August of the previous year, the higher the maximum value of the chl-a concentration. Looking at the linear regression graph it seems it could be better explained by exponential correlation (Figure 13c). It is visible that the data is more scattered than in the previous two examples. There is a higher variation especially after the sea surface temperature reaches 15^{o}C. The

average temperature for the north regions of the North Sea equals 13.86^{o}C and in the south SST reaches on average approximately 16^{o}C, with the minimum value of SST being approximetly14.55^{o}C in the summer months. It means that in the south and the central east regions there is a higher interannual variability in the peak of chl-a values during the bloom (Figure 15b). The correlation coefficient equalled $r=0.54$ for $p<0.001$. The rest of the correlations that were found to be statistically significant had relatively low values of the correlation coefficient.

However, even with a small correlation coefficient value, interestingly, a positive correlation was found between the day of SOB and the number of days this bloom lasted ($r=0.31$ for $p<0.001$). That means other factors needed to influence the number of days the bloom was present. Looking at the whole North Sea it seems that the bloom lasted shorter when the summer temperature of preceding year was higher ($r=-0.31$ for $p=0.001$). This negative correlation was also found looking at EOB ($r=-0.27$ for $p=0.006$), and PTB, although this last correlation was weak ($r=-0.20$ for $p=0.039$). Looking at temperatures of the seas surface during the winter of proceeding seasons it seems that there is weak positive correlation between SOB ($r=0.22$ for $p=0.027$), PTB ($r=0.28$ for $p=0.020$) and EOB ($r=0.20$ for $p=0.039$). Additionally, the LOB seems to last longer when the salinity in the summer of the previous year was higher ($r=0.27$ for $p=0.005$). Similar positive correlation was found in PTB ($r=0.24$ for $p=0.014$) and EOB ($r=0.27$ for $p=0.006$). It seems that salinity in winter season that preceded the bloom did not have any significant correlation except the negative correlation with the PVB ($r=-0.26$ for $p=0.007$). Additionally, SST and SSS are correlated with each other. Higher salinity corresponds with lower summer temperatures ($-0.40<r<-0.53$) and higher winter temperatures ($0.51<r<0.57$). All correlations can be found in Table 4.

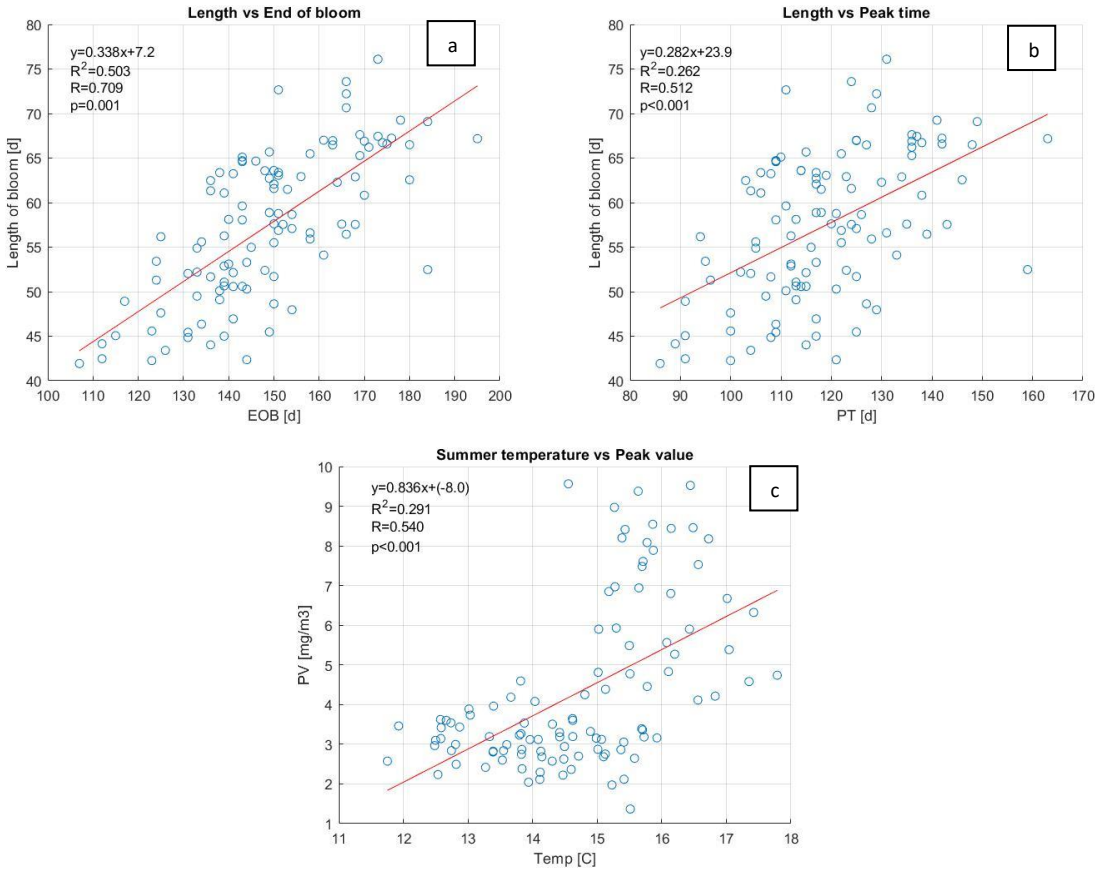

Figure 13. a. Correlation between Length of the bloom [d] and the day of year when the end of the bloom starts [d] y=0.34x+7.2, r=0.71, r^2=0.50, p<0.001. b. Correlation between Length of the bloom [d] and the time when chl-a concentration [d] reaches the highest value y=0.28x+23.9, r^2=0.26, r=0.512, p<0.001. c. Correlation between Highest value of chl-a concentration [mg/m^3] during the bloom and temperature in the summer [^{o}C] (June, July, August) months of the previous year y=0.84x-8.0, R2=0.291, r=0.54, p<0.001. Determined for the whole North Sea based on data from 2002 to 2020 (ex. 2017)

Table 4. Correlation between variables for the whole region of the North Sea using Pearson r test. Correlation coefficient numbers marked in red mean that there was different outcome in Spearman rho test.

	SOB	**PT**	**PV**	**EOB**	**L**	**T sum**	**T win**	**Sal sum**
SOB	.							
PT	0.97**	.						
PV	0.16	0.13	.					
EOB	0.89**	0.96**	0.01	.				
L	0.31**	0.51**	-0.24*	0.71**	.			
T sum	-0.16	-0.21*	0.54**	-0.27**	-0.31**	.		
T win	0.21*	0.28*	-0.06	0.20*	0.09	-0.28**	.	
Sal sum	0.19	0.24*	-0.09	0.27**	0.27**	-0.40**	0.51**	.
Sal win	0.13	0.14	-0.26**	0.14	0.11	-0.53**	0.57**	0.74**

Note ** Correlation is significant at the 0.01 level (two tailed)
* Correlation is significant at the 0.05 level (two tailed)

4.2 Characteristics of spring blooms and factors influencing them according to regions

The results for region A were the most dependable of all the study area because of the smallest number of discarded pixels. The northeast sections of region A had only one bloom season detected, however after more in depth analysis it appeared to be correct. On average for the whole time series the number of pixels that were considered during the analysis in region A (46 103km^2) was 93% per year. For region B (150 332km^2) it was approximately 72%, region C (20 143km^2) only 39%, region D (11 559km^2) which is the smallest region, located on Dogger Bank, 50%, region E (37 259km^2) approximately 68% and region F (33 803km^2) on average 70% (Figure 8) (Table 3). The missing data were pixels that needed to be discarded from the analysis due to incorrect interpretations of the bloom peaks by TIMESAT software. It was decided to discard whole region C from the correlation analysis due to too many missing values.

No statistically significant differences in spring phytoplankton bloom parameters were found between region B and D that are both located in the open water areas (Figure 14). Region E (south) and F (central east) are similar in phytoplankton bloom characteristics for the S1, except in the duration of bloom ($p<0.05$) (Figure 14f). Furthermore, the results of the Dunn-Bonferroni test show that region A differs from the rest of the regions in the bloom timing, SOB (A differs from B, D, F), PTB (A differs from all the regions), EOB (A differs from B, D, E), ($p <0.05$) (Figure 14).

On average the blooms begin at the latest in region A (Figure 15a), however there is a high interannual variation visible in all the regions in terms of beginning, peak, and start of the end of bloom. There was no change found in the timing of these parameters for the spring blooms, but there are strong correlations found between them. All regions show strong positive correlation between the day of SOB and the day of the PTB with r between 0.62 in region B and 0.90 in region E. The correlation between the day of SOB and the day of EOB has even higher correlation coefficient between 0.94 in region A and B to almost 0.96 in region E. The same strong positive correlation was found in all the regions between the day of PTB and EOB with r between 0.82 in region B to 0.98 in region E. All the above-mentioned correlations were for $p<0.001$.

Looking at the chl-a, the highest concentration through the whole time series, during the bloom was present in region E (south) and F (central east) and the lowest in region B and D (north-central) (Figure 15b). It is obvious that the PVB values differ significantly between the regions located in the north (A, B, D), the south (E) and the central east (F) (Figure 14c). When looking at the analysis of the PVB over time, in most regions the value of PVB is decreasing (Figure 15b). However, statistically significant results have been found only in regions A ($r=-0.75$ for $p<0.001$) (Figure 16a) and F ($r=-0.68$ for $p=0.002$) (Figure 16f). The only region showing an upward trend in the peak value of chl-a during the blooms in recent years is region E ($r=0.47$ for $p<0.05$) (Figure 16c). Interestingly, the results show that the later the bloom starts in the southern region the more abundant it will be ($r=0.50$ for $p<0.033$).

The duration of the bloom in the most southern region (E) is different from that of region A, D and F (Figure 14f). Additionally, the length of bloom in region A lasts longer than in region B (Figure 14f & Figure 15c). Region E is the only location which shows a decrease in the length of bloom throughout the time series ($r=-0.83$ for $p<0.001$) (Figure 16d). Moreover, region A and B show that later the start of bloom shorter it will last ($r=-0.53$ for $p<0.025$ in region A and $r=-0.63$ for $p<0.005$ in region B). It should be noted that in regions E and F, there appears to be no correlation and the onset of bloom, and the length of bloom are independent of each other. In addition, in region D, this correlation was not identified, however there was strong positive dependency between the day when the end of bloom starts ($r=0.73$ for $p<0.001$), the time of the peak ($r=0.55$ for $p=0.024$) and the length. Similarly, to region D, region F, shows a positive correlation between EOB and LOB ($r=0.52$ for $p<0.028$).

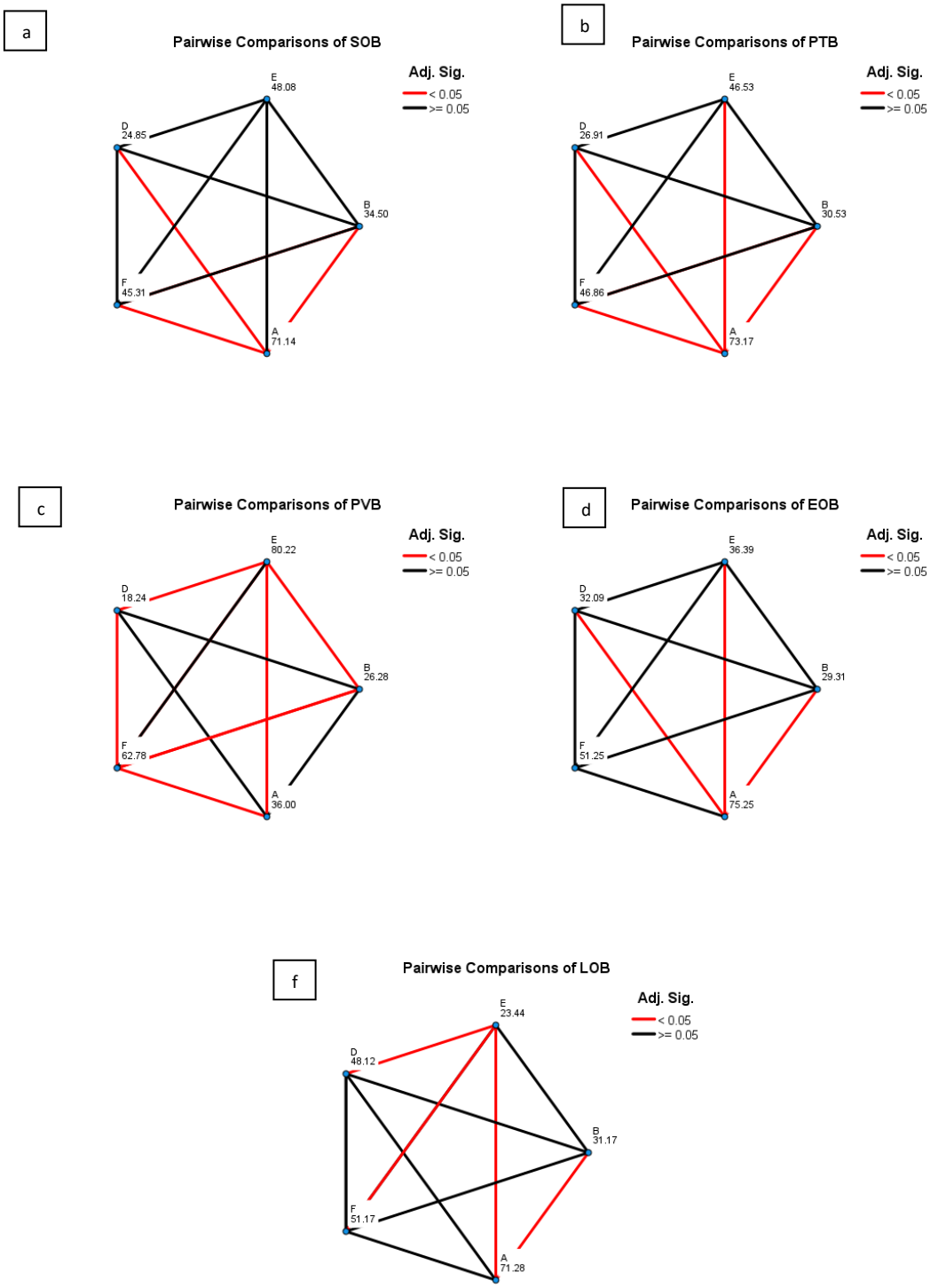

Figure 14. The statistical results of differences for the phenological parameters between the regions (red line show statistically significant differences between regions, black lines show no statistically significant differences between the regions $p<0.05$). The p value has been adjusted by Bonferroni correction for multiple tests. Each node shows the sample average rank of region.

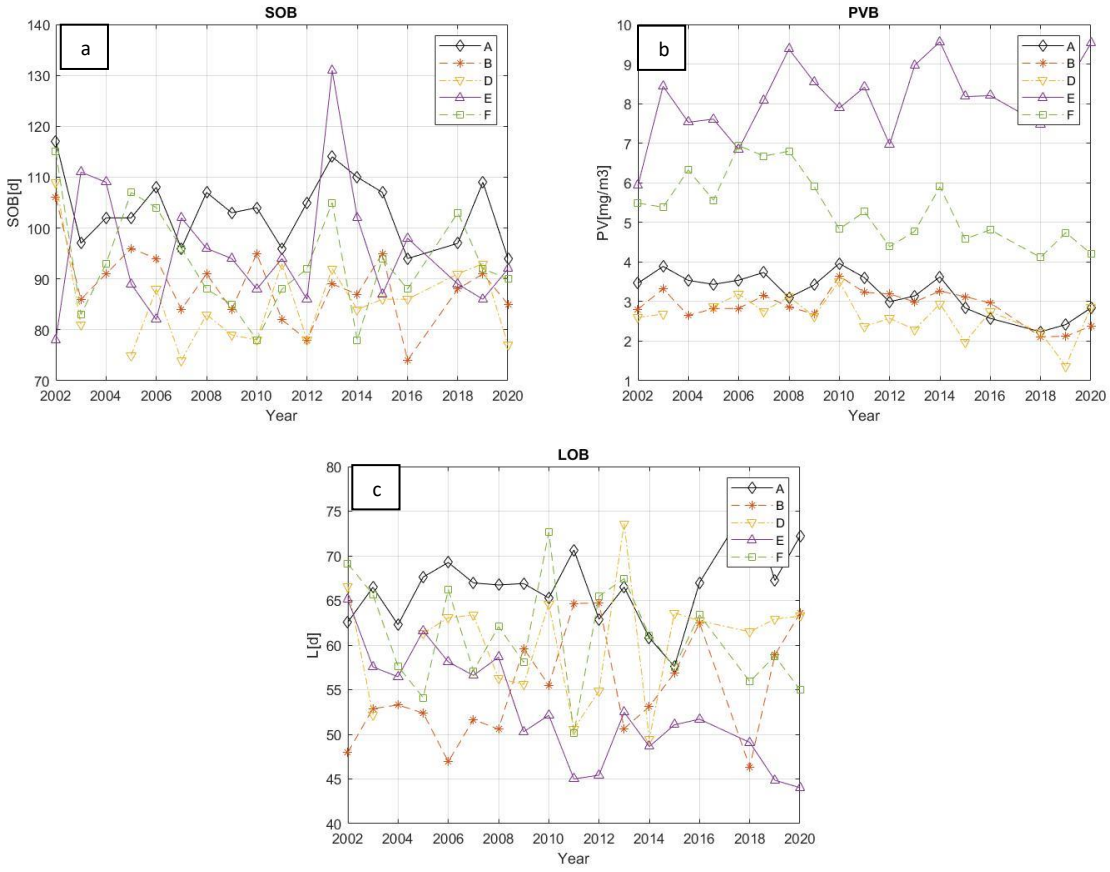

Figure 15. Parameters per region: a. day of start of bloom (SOB [d]), b. maximum value of chl-a concentration (PVB [mg/m^3]) c. number of days the bloom lasted (LOB [d]). Black line northwest region, red dash line central (open water) region, yellow dash line region dogger bank region, purple line south region, green central east region

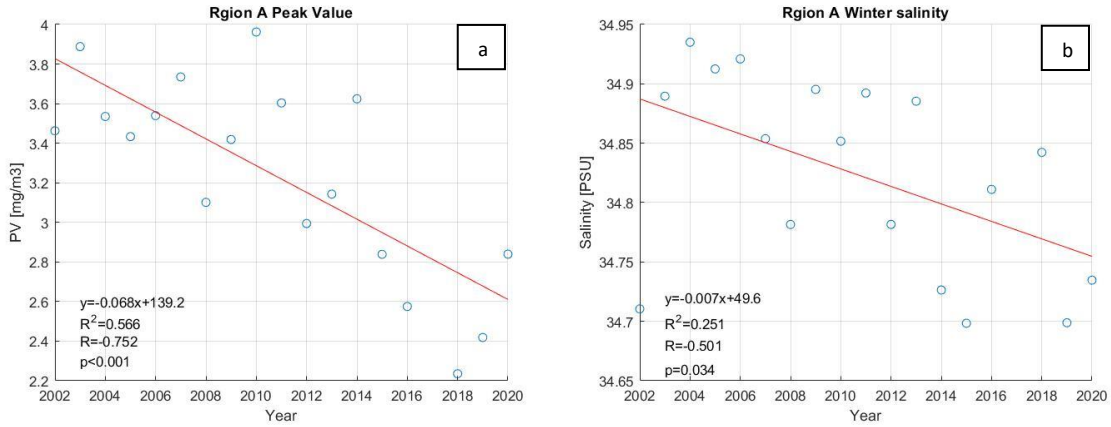

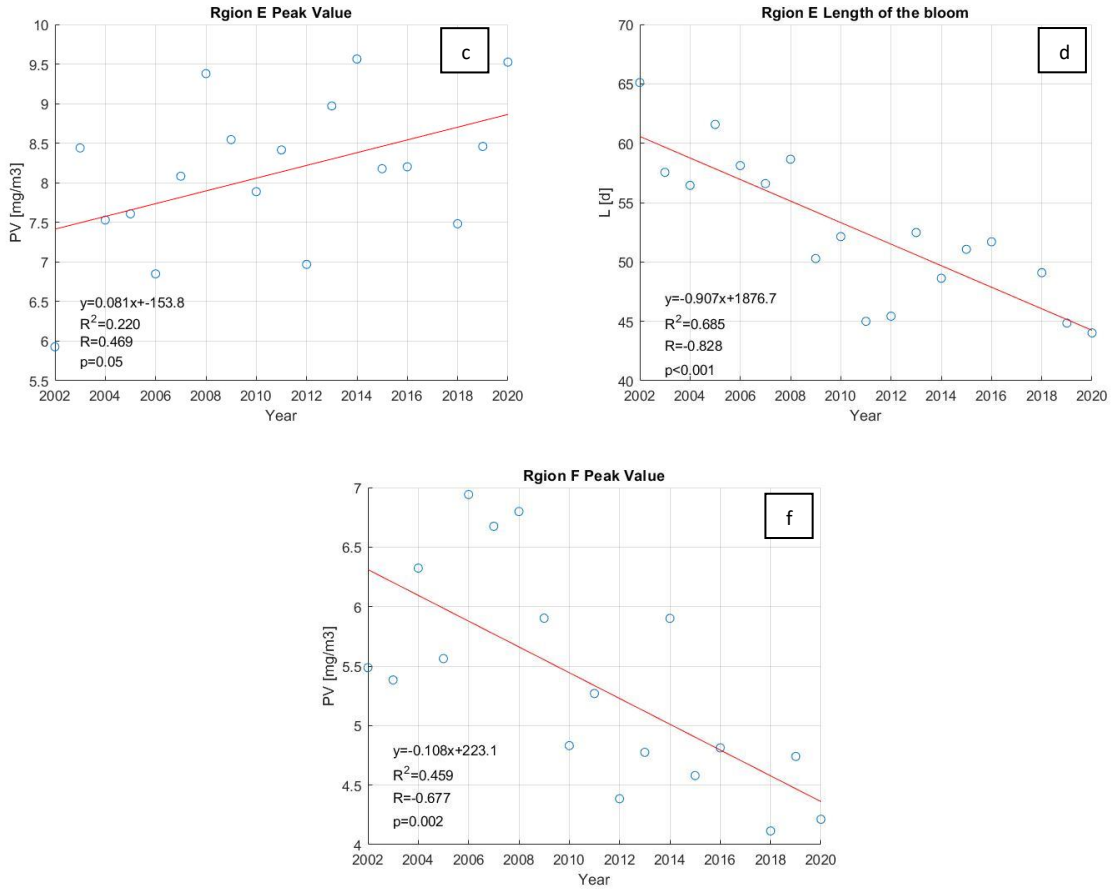

Figure 16. Statistically significant temporal trend (red line) between 2002-2020 (ex.2017) in the North Sea in different regions. a. median of the PVB [mg/m^3] in region A, b. median of sea surface salinity [PSU] in region A, c. median of the PVB [mg/m^3] in region E, d. median of the Length of the bloom [d] in region E, f. median of the PVB [mg/m^3] in region F

Impact of SST and SSS was not statistically significant for the specific regions in the North Sea, excluding region D where a significant inverse dependency on salinity in winter (r=-0.49 for p <0.048) and in summer months (r=-0.60 for p <0.010) of preceding year on SOB was present. In the same region, a negative correlation was noticed between PTB and salinity in summer months (r=-0.55 for p <0.023). Nevertheless, no statistically significant correlation was found in other regions, the relationship between bloom parameters and SST and bloom parameters and SSS is consistent in region A. It is characterized by the coldest temperatures in summer and the warmest in winter, and salinity in the summer and winter months are relatively high (Figure 17), however the salinity in winter is decreasing (r=-0.50 for p <0.034) (Figure 16b). It is also a region where the time of start, peak and end of the bloom begin the latest, and bloom duration is the longest. Region F has on average the highest temperatures in the summer, the lowest in the winter, and the salinity in winter and summer month is the lowest of all regions

due to high riverine inputs. However, it shows the biggest variability in the SST and SSS data. It is not the region where the bloom occurs the earliest and the duration of bloom is not the shortest, other factors need to influence this region. For all correlations across different regions see the Appendix.

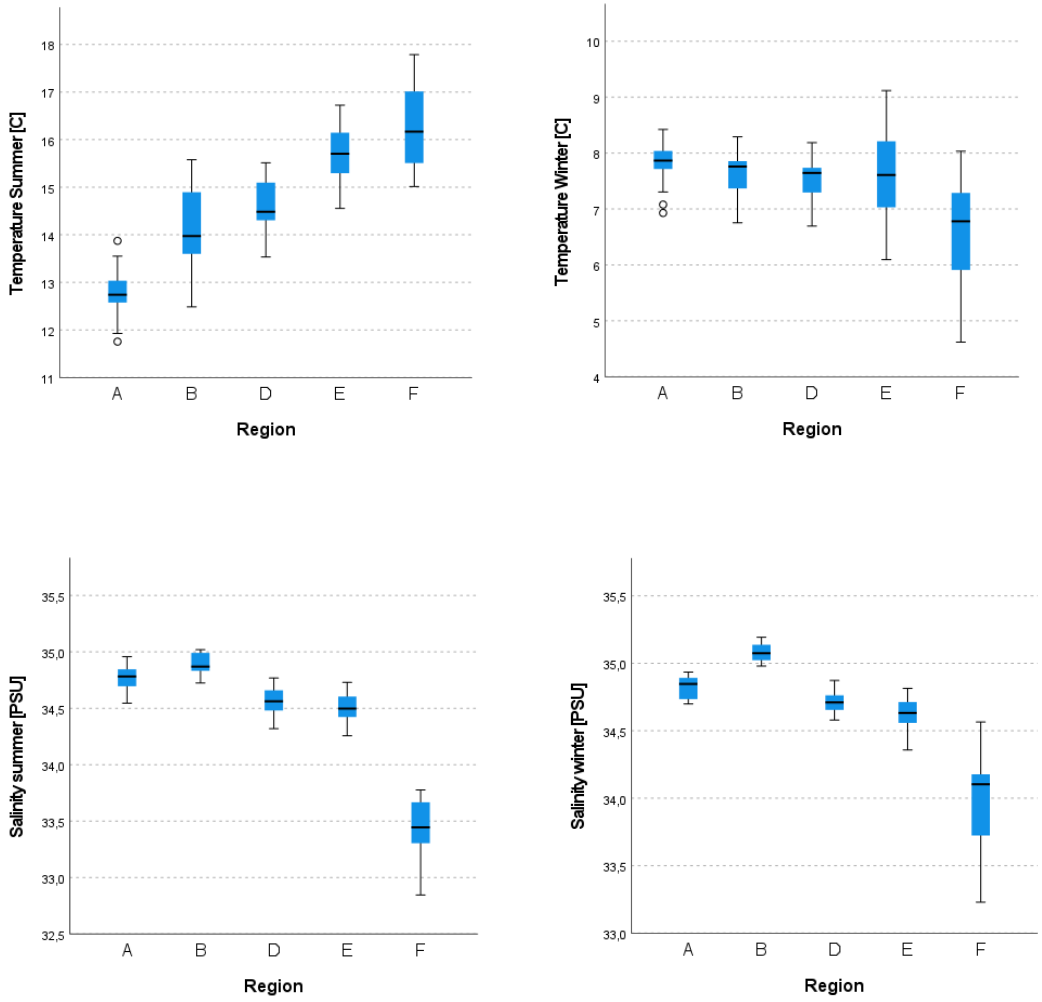

Figure 17. boxplots for each of the regions for a. summer temperatures [ºC], b. winter temperatures [ºC], c. salinity in summer months [PSU], d. salinity in winter months [PSU]

5. Discussion

This section first describes the performance of TIMESAT software in the analysis of phytoplankton blooms in the North Sea. An overview of TIMESAT effectiveness and the challenges addressed is provided. The second part of the discussion focus on the key results of the spatiotemporal analysis of spring phytoplankton bloom. The effects of SST and SSS on bloom parameters are described in details and the hypotheses formulated at the beginning of the research are referred. The results are compared with previous research done in this region.

5.1 Performance of TIMESAT software in the North Sea

In some areas the bloom patterns were too complex for TIMESAT software to recognize the peaks correctly, and as described previously in methodology, the late summer, early autumn season peak could not always be accurately recognized due to the lack of winter month data. It could be speculated that TIMESAT software might not be suitable for region D where the bloom patterns are more complicated. The water stratification has been observed only on the northern slope of Dogger Bank (Quante, M., et al. 2016) and the primary production has been reported to be present there during the whole year (Ducrotoy, J. P. et al., 2000). This was a reason why this location was selected as a separate region. During the analysis, the hypothesis was confirmed, TIMESAT was not always able to recognize the peaks in this region. This occurred because TIMESAT can analyse one or two annual seasons but in many of the pixels more than 2 bloom seasons were picked up by the software. Only 50% of the investigated pixels during spring bloom could be validated. Additionally, the percentage of correctly investigated peaks in Norwegian Trench and Skagerrak strait were too small for spring bloom resulting in discarding the whole region from the analysis.

Season 2 could not be explored using TIMESAT software in any of the regions due to insufficient number of pixels with correctly detected bloom peaks. There are several possibilities as to why this occurred. In some areas, particularly in the northern North Sea, the data was insufficient, causing TIMESAT to create artificial bloom peaks of S2 that had to be excluded later. Furthermore, it seems that the decrease in chl-a in southwest of region B, region C, east of region D and E, starts in February. Based on those results, it can be concluded that peaks of late summer, early autumn either occurred during or finished just after a period when

no satellite data was available, resulting in TIMESAT detecting only one bloom season with incorrect start and end of blooms. A recent scientific paper in which the authors also used satellite imagery data discovered similar patterns in the bloom timing of S2 in those regions, except for the southern North Sea, which was not considered (Silva, E., et al., 2021).

5.2 Average timing of spring bloom and the temporal trend

The result of this study shows that there are high interannual changes in the timing of the S1 blooms in the North Sea. No significant temporal trends were noticed in any of the study area for the investigated 17 years either for onset, peak or end of bloom. This conclusion corresponds to the outcome of the Silva, E., et al. (2021) research that did not find any significant change in the bloom timings in the open water region. Silva, E., et al. (2021) decided on excluding areas that exhibit the patterns described above as well as the southern part of the North Sea. Alternatively, Desmit, X., et al. (2020) reported that a trend toward earlier onset of spring bloom from 2000 and earlier peak time of spring bloom from 1970 is present in parts of the southern and central open waters of the North Sea. However, the result from the Desmit, X. et al. (2020) study was not confirmed by the present analysis. The reason for this could be the differences in sampling sites. Desmit, X., et al. (2020) chose mainly locations in coastal waters, no further than 20km from the land, except for a few sampling stations situated in the open waters of the North Sea. The areas close to the shoreline were excluded in this analysis. Additionally, the time series of this study considers only 17 years while Desmit, X., et al. (2020) analysis took into account a much longer period.

The outcome of this study indicates the start of bloom for the whole North Sea on 1st of April with open water region and the Dogger Bank being the regions with the earliest onset on 26th and 28th of March, respectively. The Silva, E., et al., (2021) analysis showed that on average the bloom onset started on 10th of March in open waters of the North Sea. The reason for these inconsistencies could be the different method used for the calculation of the bloom initiation values. Following the methodology of Benzouaï, S., et al. (2020) and due to TIMESAT limitations, which allows only one initiation value be used for the whole time series, it was decided to use for this study the median threshold method instead of the cumulative sum favoured by Silva, E., et al., (2021).

There are a couple of reasons why this method could overestimate the time of bloom start. Firstly, the median threshold value will be higher for longer bloom length which can cause the earlier blooms to not be discovered (Brody, S. R., et al. 2013). Secondly, the dataset was missing the relevant winter months data which may introduce bias causing the onset of the season to be shifted. According to Brody, S. R., et al. (2013) the different methods used for finding the start of bloom show same major patterns, however, in some areas using alternative methods could cause even more than 2 months disparity in bloom onset.

Contrarily, McQuatters-Gollop, et al. (2007) used the in-situ data from 1958 to 2003 to find spatial and temporal changes in diatom and dinoflagellate blooms pattern. They reported the start of bloom on average in March only in shallow waters of the North Sea and the Skagerrak strait. The deeper open waters according to McQuatters-Gollop, et al. (2007) showed the increase in diatom abundance in April. The bias that could have been introduced in this study will not affect the later correlation analysis due to the same error being present in all the years in the time series. The peak time of the S1 occurred in the beginning of May which is consistent with other studies (McQuatters-Gollop, et al. 2007, Silva, E., et al., 2021). In all the regions the bloom onset, peak time and bloom end were highly correlated.

5.3 Impact of SST and SSS on spring bloom timing

SST and SSS have moderate correlation with each other which could be explained by the inflow of Atlantic water masses. However, both parameters had mostly weak dependency ($-0.31<r<0.28$) with bloom timing in the whole region of the North Sea, but they were statistically significant ($p<0.05$). It was concluded that the warmer the SST in the previous summer, the earlier the peak time began, the earlier the bloom ended, and it had shorter duration. Winter SST had an inverse effect on phytoplankton bloom timing. Warmer winter temperatures were expected to correlate with earlier spring bloom events but surprisingly they showed correlation with later spring bloom onset. However, it led to later end of first bloom season. Salinity in the summer of the previous year showed a relationship with the later bloom onset, later end, and longer duration of the bloom itself. Winter salinity did not affect the bloom timing.

When the correlation test was performed on the chosen regions of the North Sea, SST and SSS did not show statistically significant results on bloom parameters, except for the Dogger Bank. In contrast to the weak general trend noticed in the North Sea, higher SSS partially explained

faster start of bloom in this area, which could be due to higher nutrients concentration. Additionally, in the Dogger Bank start and peak times had a moderate negative relationship with summer SST, however it was not statistically significant ($p>0.05$). This means that small-scale processes influence the timing of bloom, and the impact of SST and SSS alone are insufficient to explain variations in phytoplankton phenology. Other factors, like light availability, which was not included in this study but is a limiting factor for the bloom occurrence, could be considered as a parameter that more comprehensively explains the fluctuations in bloom timings. A decrease in water clarity due to resuspension of sediments and browning of lakes and rivers that later flow into the North Sea was reported to delay the bloom especially in coastal waters (Opdal, A. F., et al., 2019).

5.4 Average length of spring bloom and the temporal trend

The average duration of the bloom in the North Sea was determined to last 57 days, with the open water areas reaching a slightly shorter number of 55 days. This number is similar to Silva, E., et al. (2021) findings that reported the length of the bloom to be on average 46 days in the deep North Sea open waters. The estimated duration value is comparable, especially considering that the data used for this analysis was binned in 8-day averages.

No significant temporal change in bloom duration was observed in most of the study area. The exception was the south region, which showed a decrease throughout the years. The bloom duration depended on when the bloom started and ended in the year. The blooms that start earlier are reported to have slower growth and because of that they should generally last longer (van Beusekom, J. E., & Diel-Christiansen, S, 2009). The late bloom onset resulted in a shorter bloom duration in the northern regions. The southern areas, together with the Dogger Bank, exhibited longer bloom duration when peak day and end of bloom happened later in the year and the length was independent from the start of bloom. As mentioned previously, the bloom onset during this study could be overestimated which may be a reason why this correlation was not found in some of the study areas. Region located along the Scottish coast, with high saline waters due to the proximity of the Atlantic Ocean, the coldest temperatures in the summer and warmest in the winter, was characterized by the latest, but longest blooms compare to other areas.

5.5 Average chl-a maximum value of spring bloom and the temporal trend

Chl-a maximum in the northern and central areas including the Dogger Bank reach on average 2.9 mg/m^3 while in the southern regions the value is much higher, approximately 6.7 mg/m^3. The peak values of chl-a have significant differences between the north and the south and the central east regions of the North Sea with the south coming to much higher values. The reason for that is the higher concentration of nutrients in the south coastal waters, which are delivered by the riverine input. The amount of nutrients present in the open waters of the North Sea is significantly smaller (van Beusekom, J. E., & Diel-Christiansen, S., 2009).

Nevertheless, confidence levels for chl-a concentrations in the southern and the central eastern regions of the North Sea are low. The maximum value of chl-a may be overestimated in the south due to estimation with Case 1 water data. More reliable results could be achieved by using the algorithm for Case 2 water in these regions. However, mean chl-a concentrations in the south from 2015 to 2019 have been reported to exceed 6 mg/m^3 in coastal areas and reach values between 3–6 mg/m^3 further away from the coast (EEA, 2022). This corresponds to the values calculated during this analysis. The south was the only area where an increase in chl-a maximum during the peak time was visible while the general trend showed a decrease with statistically significant results at region level along the Scottish coast and in the central east area between the Netherlands, Germany, and Denmark.

5.6 Impact of SST and SSS on spring chl-a maximum value

Warmer summer SST showed a moderate correlation (r=0.54) with chl-a maximum values during the peak and thus may be a potential environmental factor explaining the spring bloom intensity. Higher abundance of chl-a during the warm periods and smaller blooms during the cold events are known and reported in the North Sea (Alvarez-Fernandez, S. et al., 2012). The potential explanation of this correlation could be that warmer SST increases phytoplankton growth (Bissinger, J. E., et al. 2008) and it could cause chl-a concentration to reach higher values. In the open water warmer SST could also influence the formation of thermocline that keeps nutrients and phytoplankton in well-lightened upper layer allowing the bloom to accelerate (Quante, M., et al. 2016). However, once nutrients are depleted, strong thermocline would not allow for their replenishment and the bloom will finish.

The earlier bloom end and its shorter duration during higher SST leads to the conclusion that higher temperatures in summer months could cause an early end of the season due to increased intensity of the bloom. However, looking at the North Sea at a regional level, there was no obvious relationship between winter SST or SSS and chl-a concentration values. The Scottish coast region was the only area that showed the decrease of winter salinity likely caused by lower Atlantic inflow. This could mean a lower input of nutrients in this section which could explain lower chl-a maximum. The decline in riverine nutrients input noticed from 1980s (Desmit, X., et al., 2020) could impact the decrease in chl-a concentration and phytoplankton primary production (Capuzzo, E., et al., 2018) in central east region.

6. Summary and conclusion

The data for years 1998 to 2001, when ocean reflectance data was only supplied by SeaWiFS sensor, was excluded from the analysis due to poor coverage and as a result, a large number of missing values. A series of satellite data from 2002 to 2020, excluding the year 2017 due to data unavailability, was analysed to examine possible trends in the intensity of phytoplankton blooms and a shift in their occurrence. The impact of the SST and SSS fluctuations on the bloom patterns were the matter of investigation. In the end only spring bloom analysis was performed. The second phytoplankton bloom could not be analysed due to data being available only from February to October which in some regions led to a misinterpretation of the bloom season. Additionally, the analysis of spring bloom was not possible for all regions. Norwegian Trench and Skagerrak strait region was discarded due to too many pixels with incorrectly recognized spring bloom.

In conclusion, no shift in spring bloom timings and duration, except shorter duration in southern region, was discovered in the North Sea during the investigated time series. Only weak dependency on sea surface temperature and salinity was identified, except in the Dogger Bank region, where higher sea surface salinity was responsible for faster bloom occurrence, but it was not highly correlated in other sectors. This result disproves the formulated hypothesis of an earlier start and peak day and longer duration of spring bloom. However, the start of spring bloom should be further investigated due to possible overestimation of bloom onset which could have been introduced in the data by using the median threshold method for finding the bloom initiation values**.**

The general trend of blooms intensity, during first bloom, in the North Sea showed a decrease throughout the years. Based on the analysis, sea surface temperature was found to be a potential factor impacting the levels of chl-a concentration in the research area, showing an increase in chl-a maximum values with higher SST. Nevertheless, it was not enough to explain the fluctuations in specific regions, therefore, more detailed research is required. Additionally, further investigation into fluctuations of chl-a concentration in southern regions using the data for Case 2 waters should be performed due to possible overestimation of values during this study by the usage of data for Case 1 waters. The late spring, early autumn bloom could not be analysed, and more research should be done in the future to explore possible shift in the timings,

duration, chl-a concentration of second bloom season and their dependency on environmental drivers.

The North Sea has complex hydrological characteristics, influenced by the NAO-dependent Atlantic water influx and riverine inputs. Evaluating the results of the analysis of the whole North Sea and separate regions respectively, it can be concluded that there are significant differences between them. The local factors have influence over the phytoplankton phenology. To bring a broader perspective to this area, it would be beneficial to perform more detailed analysis of the North Sea by considering the unique environmental processes in specific locations. More environmental drivers that were not considered during this study, for example light availability, winds, turbidity, mixed layer depth or zooplankton grazing could be responsible for the changes in bloom dynamics. The existing research on phytoplankton bloom fluctuations that takes into consideration many different drivers are focused only on specific parts of the North Sea. The potential study gap can be explored, as there are not enough resources about the North Sea as a whole ecosystem.

7. References

Alvarez-Fernandez, S., Lindeboom, H., & Meesters, E. (2012). Temporal changes in plankton of the North Sea: community shifts and environmental drivers. *Marine Ecology Progress Series*, *462*, 21-38.

Barcelos e Ramos, J., Schulz, K. G., Voss, M., Narciso, Á., Müller, M. N., Reis, F. V., ... & Azevedo, E. B. (2017). Nutrient-specific responses of a phytoplankton community: a case study of the North Atlantic Gyre, Azores. *Journal of Plankton Research*, *39*(4), 744-761.

Benzouaï, S., Louanchi, F., & Smara, Y. (2020). Phytoplankton phenology in Algerian continental shelf and slope waters using remotely sensed data. *Estuarine, Coastal and Shelf Science*, *247*, 107070.

Bissinger, J. E., Montagnes, D. J., harples, J., & Atkinson, D. (2008). Predicting marine phytoplankton maximum growth rates from temperature: Improving on the Eppley curve using quantile regression. *Limnology and Oceanography*, *53*(2), 487-493.

Bock, N., Subramaniam, A., Juhl, A. R., Montoya, J., & Duhamel, S. (2022). Quantifying Per-Cell Chlorophyll a in Natural Picophytoplankton Populations Using Fluorescence-Activated Cell Sorting.

Brody, S. R., Lozier, M. S., & Dunne, J. P. (2013). A comparison of methods to determine phytoplankton bloom initiation. *Journal of Geophysical Research: Oceans*, *118*(5), 2345-2357.

Cai, Z., Jönsson, P., Jin, H., & Eklundh, L. (2017). Performance of smoothing methods for reconstructing NDVI time-series and estimating vegetation phenology from MODIS data. *Remote Sensing*, *9*(12), 1271.

Capuzzo, E., Lynam, C. P., Barry, J., Stephens, D., Forster, R. M., Greenwood, N., ... & Engelhard, G. H. (2018). A decline in primary production in the North Sea over 25 years, associated with reductions in zooplankton abundance and fish stock recruitment. *Global change biology*, *24*(1), e352-e364.

Claussen, U., Zevenboom, W., Brockmann, U., Topcu, D., & Bot, P. (2009). Assessment of the eutrophication status of transitional, coastal, and marine waters within OSPAR. In *Eutrophication in Coastal Ecosystems* (pp. 49-58). Springer, Dordrecht.

d'Andon, O. F., Antoine, D., Mangin, A., Maritorena, S., Durand, D., Pradhan, Y., ... & Barrot, G. (2008). Ocean colour sensors characterisation and expected error estimates of ocean colour merged products from GlobColour. In *Proceedings ocean optics XIX, Barga, Italy, October 6–10* (p. 51).

Darecki, M., Weeks, A., Sagan, S., Kowalczuk, P., & Kaczmarek, S. (2003). Optical characteristics of two contrasting Case 2 waters and their influence on remote sensing algorithms. *Continental Shelf Research*, *23*(3-4), 237-250.

Desmit, X., Nohe, A., Borges, A. V., Prins, T., De Cauwer, K., Lagring, R., ... & Sabbe, K. (2020). Changes in chlorophyll concentration and phenology in the North Sea in relation to de-eutrophication and sea surface warming. *Limnology and Oceanography*, *65*(4), 828-847.

Desmit, X., Ruddick, K., & Lacroix, G. (2015). Salinity predicts the distribution of chlorophyll a spring peak in the southern North Sea continental waters. *Journal of Sea Research*, *103*, 59-74.

Driscoll, W. C. (1996). Robustness of the ANOVA and Tukey-Kramer statistical tests. *Computers & Industrial Engineering*, *31*(1-2), 265-268.

Ducrotoy, J. P., Elliott, M., & de Jonge, V. N. (2000). The North Sea. *Marine pollution bulletin*, *41*(1-6), 5-23.

Eklundh, L., & Jönsson, P. (2017). TIMESAT 3.3 with seasonal trend decomposition and parallel processing Software Manual.

Eleveld, M. A., Van Der Woerd, H. J., & Beck, H. (2007, April). Improving the estimation of North Sea primary production: Meris chl and kd in vgpm. In *Envisat Symposium* (Vol. 2007).

European Environment Agency, (2022) *Chlorophyll in transitional, coastal and marine waters in Europe*

Falkowski, P. G., Laws, E. A., Barber, R. T., & Murray, J. W. (2003). Phytoplankton and their role in primary, new, and export production. In *Ocean biogeochemistry* (pp. 99-121). Springer, Berlin, Heidelberg.

Fettweis, M., Baeye, M., Van der Zande, D., Van den Eynde, D., & Joon Lee, B. (2014). Seasonality of floc strength in the southern North Sea. *Journal of Geophysical Research: Oceans*, *119*(3), 1911-1926.

Flemming, N. C., Harff, J., Moura, D., Burgess, A., & Bailey, G. N. (Eds.). (2017). *Submerged landscapes of the European continental shelf: Quaternary paleoenvironments* (Vol. 1). John Wiley & Sons.

Garrison, T. S. (2012). *Oceanography: an invitation to marine science*. Cengage Learning.

Gohin, F., Bryère, P., Lefebvre, A., Sauriau, P. G., Savoye, N., Vantrepotte, V., ... & Rétho, M. (2020). Satellite and in situ monitoring of Chl-a, Turbidity, and Total Suspended Matter in coastal waters: experience of the year 2017 along the French Coasts. *Journal of Marine Science and Engineering*, *8*(9), 665.

How much oxygen comes from the ocean? https://oceanservice.noaa.gov/facts/ocean-oxygen.html, 02/26/21

Høyer, J. L., & Karagali, I. (2016). Sea surface temperature climate data record for the North Sea and Baltic Sea. *Journal of Climate*, *29*(7), 2529-2541.

International Ocean Colour Coordinating Group [IOCCG] (2007). Ocean-Color Data Merging. Dartmouth, NS: IOCCG.

Koul, V., Schrum, C., Düsterhus, A., & Baehr, J. (2019). Atlantic inflow to the North Sea modulated by the subpolar gyre in a historical simulation with MPI-ESM. *Journal of Geophysical Research: Oceans*, *124*(3), 1807-1826.

Leeuw, T., Boss, E. S., & Wright, D. L. (2013). In situ measurements of phytoplankton fluorescence using low cost electronics. *Sensors*, *13*(6), 7872-7883.

Leterme, S. C., Pingree, R. D., Skogen, M. D., Seuront, L., Reid, P. C., & Attrill, M. J. (2008). Decadal fluctuations in North Atlantic water inflow in the North Sea between 1958-2003: impacts on temperature and phytoplankton populations. *Oceanologia*, *50*(1), 59-72.

Maritorena, S., & Siegel, D. A. (2005). Consistent merging of satellite ocean color data sets using a bio-optical model. *Remote Sensing of Environment*, *94*(4), 429-440.

Martinez, E., Antoine, D., d'Ortenzio, F., & de Boyer Montégut, C. (2011). Phytoplankton spring and fall blooms in the North Atlantic in the 1980s and 2000s. *Journal of Geophysical Research: Oceans*, *116*(C11).

McQuatters-Gollop, A., Raitsos, D. E., Edwards, M., & Attrill, M. J. (2007). Spatial patterns of diatom and dinoflagellate seasonal cycles in the NE Atlantic Ocean. *Marine Ecology Progress Series*, *339*, 301-306.

Mobley, C. D., Stramski, D., Paul Bissett, W., & Boss, E. (2004). Optical modeling of ocean waters: Is the case 1-case 2 classification still useful?. *Oceanography*, *17*(SPL. ISS. 2), 60.

Morán, X. A. G., López-Urrutia, Á. N. G. E. L., Calvo-Díaz, A. L. E. J. A. N. D. R. A., & Li, W. K. (2010). Increasing importance of small phytoplankton in a warmer ocean. *Global Change Biology*, *16*(3), 1137-1144.

Moreno, Á., García-Haro, F. J., Martínez, B., & Gilabert, M. A. (2014). Noise reduction and gap filling of fAPAR time series using an adapted local regression filter. *Remote Sensing*, *6*(9), 8238-8260.

Opdal, A. F., Lindemann, C., & Aksnes, D. L. (2019). Centennial decline in North Sea water clarity causes strong delay in phytoplankton bloom timing. *Global Change Biology*, *25*(11), 3946-3953.

Ostertagova, E., Ostertag, O., & Kováč, J. (2014). Methodology and application of the Kruskal-Wallis test. In *Applied Mechanics and Materials* (Vol. 611, pp. 115-120). Trans Tech Publications Ltd.

Otto, L., Zimmerman, J. T. F., Furnes, G. K., Mork, M., Saetre, R., & Becker, G. (1990). Review of the physical oceanography of the North Sea. *Netherlands journal of sea research*, *26*(2-4), 161-238.

Pachiappan, P., Santhanam, P., Begum, A., & Balaji Prasath, B. (2019). An introduction to plankton. In *Basic and applied phytoplankton biology* (pp. 1-24). Springer, Singapore.

Peperzak, L. (2005). Future increase in harmful algal blooms in the North Sea due to climate change. *Water Science and Technology, 51*(5), 31-36.

Peters, S. W. M., Eleveld, M., Pasterkamp, R., Van der Woerd, H., Devolder, M., Jans, S., ... & Aas, E. (2005). Atlas of Chlorophyll-a concentration for the North Sea based on MERIS imagery of 2003. *Vrije Universiteit, Amsterdam*.

GlobColour Product User's Guide (30/03/2020), Version 4.2.1

Quante, M., Colijn, F., Bakker, J. P., Härdtle, W., Heinrich, H., Lefebvre, C., ... & Tölle, M. H. (2016). Introduction to the Assessment—Characteristics of the Region. In *North Sea region climate change assessment* (pp. 1-52). Springer, Cham.

Reid, P. C., Lancelot, C., Gieskes, W. W. C., Hagmeier, E., & Weichart, G. (1990). Phytoplankton of the North Sea and its dynamics: a review. *Netherlands Journal of Sea Research, 26*(2-4), 295-331.

Reynolds, C. S. (2006). *The ecology of phytoplankton*. Cambridge University Press.

Riebesell, U., & Wolf-Gladrow, D. A. (2002). Supply and uptake of inorganic nutrients. *Phytoplankton productivity: carbon assimilation in marine and freshwater ecosystems*, 109-140.

Santhanam, P., Begum, A., & Pachiappan, P. (Eds.). (2019). *Basic and applied phytoplankton biology*. Singapore: Springer.

Siegel, D. A., Doney, S. C., & Yoder, J. A. (2002). The North Atlantic spring phytoplankton bloom and Sverdrup's critical depth hypothesis. *science*, *296*(5568), 730-733.

Silva, E., Counillon, F., Brajard, J., Korosov, A., Pettersson, L. H., Samuelsen, A., & Keenlyside, N. (2021). Twenty-One Years of Phytoplankton Bloom Phenology in the Barents, Norwegian, and North Seas.

Siswanto, E. (2020). Temporal variability of satellite-retrieved chlorophyll-a data in Arctic and subarctic ocean regions within the past two decades. International Journal of Remote Sensing, 41(19), 7427-7445.

Statistics in focus Agriculture and fisheries Eurostat 2009

Šmejkalová, T., Edwards, M. E., & Dash, J. (2016). Arctic lakes show strong decadal trend in earlier spring ice-out. *Scientific reports, 6*(1), 1-8.

Tilman, D., Kilham, S. S., & Kilham, P. (1982). Phytoplankton community ecology: the role of limiting nutrients. *Annual review of Ecology and Systematics, 13*, 349-372.

van Beusekom, J. E., & Diel-Christiansen, S. (2009). Global change and the biogeochemistry of the North Sea: the possible role of phytoplankton and phytoplankton grazing. *International Journal of Earth Sciences, 98*(2), 269-280

van der Molen, J., & Pätsch, J. (2022). An overview of Atlantic forcing of the North Sea with focus on oceanography and biogeochemistry. *Journal of Sea Research*, 102281.

Wasmund, N., Nausch, G., Gerth, M., Busch, S., Burmeister, C., Hansen, R., & Sadkowiak, B. (2019). Extension of the growing season of phytoplankton in the western Baltic Sea in response to climate change. Marine Ecology Progress Series, 622, 1-16.

Wilson, R. J., & Heath, M. R. (2019). Increasing turbidity in the North Sea during the 20th century due to changing wave climate. *Ocean Science*, *15*(6), 1615-1625.

Wiltshire, K. H., & Manly, B. F. (2004). The warming trend at Helgoland Roads, North Sea: phytoplankton response. *Helgoland Marine Research*, *58*(4), 269-273.

Winther, N. G., & Johannessen, J. A. (2006). North Sea circulation: Atlantic inflow and its destination. *Journal of Geophysical Research: Oceans*, *111*(C12).

Wirtz, K., & Smith, S. L. (2020). Vertical migration by bulk phytoplankton sustains biodiversity and nutrient input to the surface ocean. *Scientific reports*, *10*(1), 1-12.

8. Appendix

1. Programs used in GDAL library during the analysis:
   - gdalinfo – to get information about the raster dataset.
   - gdal_translate – to convert raster data to different format and perform other operations for example resampling (Table1).
   - gdal_calc.py – to perform calculations on raster dataset.

2. Correlation per region

Table1. Region A – Northeast (along Scottish coast)

	SOB	**PT**	**PV**	**EOB**	**L**	**T sum**	**T win**	**Sal sum**
SOB	.							
PT	0.94**	.						
PV	0.08	-0.30	.					
EOB	0.79**	0.91**	0.14	.				
L	-0.53*	-0.25	-0.30	0.11	.			
T sum	-0.05	-0.12	0.22	-0.28	-0.29	.		
T win	0.01	-0.18	0.11	-0.28	-0.41	0.24	.	
Sal sum	0.20	-0.08	0.44	0.00	0.32	-0.09	-0.14	.
Sal win	-0.32	-0.23	0.46	-0.14	0.34	-0.16	-0.26	0.74**

Table2. Region B – Central (Open waters)

	SOB	**PT**	**PV**	**EOB**	**L**	**T sum**	**T win**	**Sal sum**
SOB	.							
PT	0.94**	.						
PV	-0.09	-0.21	.					
EOB	0.62**	0.82**	0.02	.				
L	-0.63**	-0.37	-0.12	0.22	.			
T sum	0.28	0.28	-0.10	0.22	-0.12	.		
T win	0.19	0.21	-0.24	0.06	-0.20	0.17	.	
Sal sum	-0.02	-0.02	-0.14	0.00	0.02	0.06	0.34	.
Sal win	-0.19	0.18	0.14	-0.31	-0.08	-0.14	-0.04	0.25

Table3. Region D – Dogger Bank

	SOB	**PT**	**PV**	**EOB**	**L**	**T sum**	**T win**	**Sal sum**
SOB	.							
PT	0.93**	.						
PV	-0.42	-0.34	.					
EOB	0.85**	0.96**	-0.38	.				
L	0.26	0.55*	-0.13	0.73**	.			
T sum	-0.45	0.47	-0.38	-0.38	-0.12	.		
T win	-0.05	0.11	-0.02	0.05	0.16	0.10	.	
Sal sum	-0.60	-0.55*	0.32	-0.40	0.06	0.15	-0.48	.

Sal win	-0.49	-0.40	0.28	-0.39	-0.07	0.07	-0.14	0.72**

Table4. Region E – South (between coast of England, The Netherlands, Belgium, and France till the English Channel)

	SOB	**PT**	**PV**	**EOB**	**L**	**T sum**	**T win**	**Sal sum**
SOB	.							
PT	0.96**	.						
PV	0.50*	0.37	.					
EOB	0.90**	0.98**	0.25	.				
L	0.00	0.26	-0.46	0.43	.			
T sum	-0.05	-0.07	0.09	-0.08	-0.12	.		
T win	0.06	0.06	0.19	0.09	0.11	0.06	.	
Sal sum	0.41	0.42	0.21	0.40	0.03	-0.08	0.08	.
Sal win	0.03	-0.02	0.23	-0.08	-0.24	-0.12	0.47	0.68**

Table5. Region F – Central east (between coast of Denmark, Germany, and The Netherlands)

	SOB	**PT**	**PV**	**EOB**	**L**	**T sum**	**T win**	**Sal sum**
SOB	.							
PT	0.96**	.						
PV	0.02	0.04	.					
EOB	0.86**	0.96**	0.04	.				
L	0.00	0.25	0.03	0.52*	.			
T sum	-0.08	-0.14	-0.02	-0.29	-0.44	.		
T win	0.19	0.19	0.08	0.09	-0.15	0.08	.	
Sal sum	-0.21	-0.21	-0.24	-0.17	0.02	0.03	0.19	.
Sal win	0.06	0.08	-0.16	0.15	0.18	-0.30	0.34	0.42

3. Setting file for northeast region:

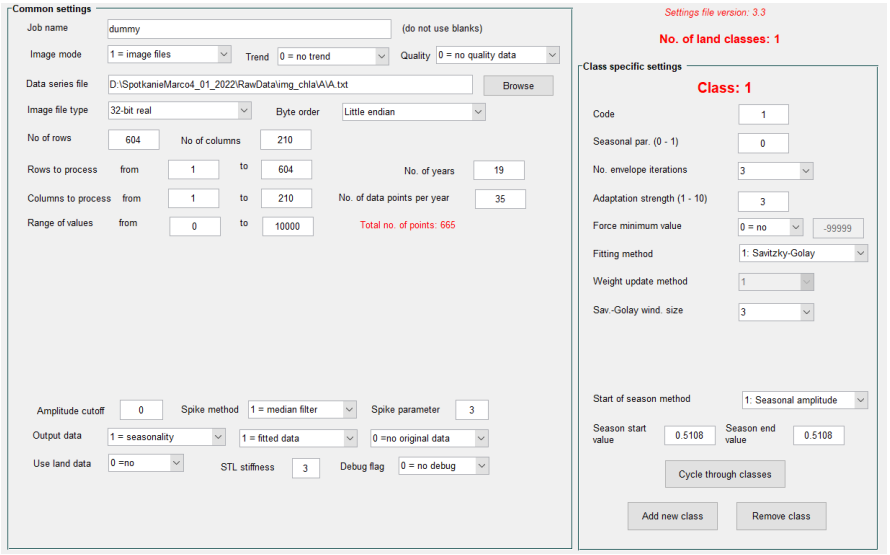

Series from Lund University

Department of Physical Geography and Ecosystem Science

Master Thesis in Geographical Information Science

1. *Anthony Lawther:* The application of GIS-based binary logistic regression for slope failure susceptibility mapping in the Western Grampian Mountains, Scotland (2008).
2. *Rickard Hansen:* Daily mobility in Grenoble Metropolitan Region, France. Applied GIS methods in time geographical research (2008).
3. *Emil Bayramov:* Environmental monitoring of bio-restoration activities using GIS and Remote Sensing (2009).
4. *Rafael Villarreal Pacheco:* Applications of Geographic Information Systems as an analytical and visualization tool for mass real estate valuation: a case study of Fontibon District, Bogota, Columbia (2009).
5. *Siri Oestreich Waage:* a case study of route solving for oversized transport: The use of GIS functionalities in transport of transformers, as part of maintaining a reliable power infrastructure (2010).
6. *Edgar Pimiento:* Shallow landslide susceptibility – Modelling and validation (2010).
7. *Martina Schäfer:* Near real-time mapping of floodwater mosquito breeding sites using aerial photographs (2010).
8. *August Pieter van Waarden-Nagel:* Land use evaluation to assess the outcome of the programme of rehabilitation measures for the river Rhine in the Netherlands (2010).
9. *Samira Muhammad:* Development and implementation of air quality data mart for Ontario, Canada: A case study of air quality in Ontario using OLAP tool. (2010).
10. *Fredros Oketch Okumu*: Using remotely sensed data to explore spatial and temporal relationships between photosynthetic productivity of vegetation and malaria transmission intensities in selected parts of Africa (2011).
11. *Svajunas Plunge:* Advanced decision support methods for solving diffuse water pollution problems (2011).
12. *Jonathan Higgins:* Monitoring urban growth in greater Lagos: A case study using GIS to monitor the urban growth of Lagos 1990 - 2008 and produce future growth prospects for the city (2011).
13. *Mårten Karlberg:* Mobile Map Client API: Design and Implementation for Android (2011).

14. *Jeanette McBride:* Mapping Chicago area urban tree canopy using color infrared imagery (2011).

15. *Andrew Farina:* Exploring the relationship between land surface temperature and vegetation abundance for urban heat island mitigation in Seville, Spain (2011).

16. *David Kanyari*: Nairobi City Journey Planner: An online and a Mobile Application (2011).

17. *Laura V. Drews:* Multi-criteria GIS analysis for siting of small wind power plants - A case study from Berlin (2012).

18. *Qaisar Nadeem:* Best living neighborhood in the city - A GIS based multi criteria evaluation of ArRiyadh City (2012).

19. *Ahmed Mohamed El Saeid Mustafa:* Development of a photo voltaic building rooftop integration analysis tool for GIS for Dokki District, Cairo, Egypt (2012).

20. *Daniel Patrick Taylor*: Eastern Oyster Aquaculture: Estuarine Remediation via Site Suitability and Spatially Explicit Carrying Capacity Modeling in Virginia's Chesapeake Bay (2013).

21. *Angeleta Oveta Wilson:* A Participatory GIS approach to *unearthing* Manchester's Cultural Heritage '*gold mine'* (2013).

22. *Ola Svensson:* Visibility and Tholos Tombs in the Messenian Landscape: A Comparative Case Study of the Pylian Hinterlands and the Soulima Valley (2013).

23. *Monika Ogden:* Land use impact on water quality in two river systems in South Africa (2013).

24. *Stefan Rova:* A GIS based approach assessing phosphorus load impact on Lake Flaten in Salem, Sweden (2013).

25. *Yann Buhot:* Analysis of the history of landscape changes over a period of 200 years. How can we predict past landscape pattern scenario and the impact on habitat diversity? (2013).

26. *Christina Fotiou:* Evaluating habitat suitability and spectral heterogeneity models to predict weed species presence (2014).

27. *Inese Linuza:* Accuracy Assessment in Glacier Change Analysis (2014).

28. *Agnieszka Griffin:* Domestic energy consumption and social living standards: a GIS analysis within the Greater London Authority area (2014).

29. *Brynja Guðmundsdóttir:* Detection of potential arable land with remote sensing and GIS - A Case Study for Kjósarhreppur (2014).

30. *Oleksandr Nekrasov:* Processing of MODIS Vegetation Indices for analysis of agricultural droughts in the southern Ukraine between the years 2000-2012 (2014).

31. *Sarah Tressel:* Recommendations for a polar Earth science portal in the context of Arctic Spatial Data Infrastructure (2014).

32. *Caroline Gevaert:* Combining Hyperspectral UAV and Multispectral Formosat-2 Imagery for Precision Agriculture Applications (2014).

33. *Salem Jamal-Uddeen:* Using GeoTools to implement the multi-criteria evaluation analysis - weighted linear combination model (2014).

34. *Samanah Seyedi-Shandiz:* Schematic representation of geographical railway network at the Swedish Transport Administration (2014).

35. *Kazi Masel Ullah:* Urban Land-use planning using Geographical Information System and analytical hierarchy process: case study Dhaka City (2014).

36. *Alexia Chang-Wailing Spitteler:* Development of a web application based on MCDA and GIS for the decision support of river and floodplain rehabilitation projects (2014).

37. *Alessandro De Martino:* Geographic accessibility analysis and evaluation of potential changes to the public transportation system in the City of Milan (2014).

38. *Alireza Mollasalehi:* GIS Based Modelling for Fuel Reduction Using Controlled Burn in Australia. Case Study: Logan City, QLD (2015).

39. *Negin A. Sanati:* Chronic Kidney Disease Mortality in Costa Rica; Geographical Distribution, Spatial Analysis and Non-traditional Risk Factors (2015).

40. *Karen McIntyre:* Benthic mapping of the Bluefields Bay fish sanctuary, Jamaica (2015).

41. *Kees van Duijvendijk:* Feasibility of a low-cost weather sensor network for agricultural purposes: A preliminary assessment (2015).

42. *Sebastian Andersson Hylander:* Evaluation of cultural ecosystem services using GIS (2015).

43. *Deborah Bowyer:* Measuring Urban Growth, Urban Form and Accessibility as Indicators of Urban Sprawl in Hamilton, New Zealand (2015).

44. *Stefan Arvidsson:* Relationship between tree species composition and phenology extracted from satellite data in Swedish forests (2015).

45. *Damián Giménez Cruz*: GIS-based optimal localisation of beekeeping in rural Kenya (2016).

46. *Alejandra Narváez Vallejo:* Can the introduction of the topographic indices in LPJ-GUESS improve the spatial representation of environmental variables? (2016).

47. *Anna Lundgren:* Development of a method for mapping the highest coastline in Sweden using breaklines extracted from high resolution digital elevation models (2016).

48. *Oluwatomi Esther Adejoro:* Does location also matter? A spatial analysis of social achievements of young South Australians (2016).

49. *Hristo Dobrev Tomov:* Automated temporal NDVI analysis over the Middle East for the period 1982 - 2010 (2016).

50. *Vincent Muller:* Impact of Security Context on Mobile Clinic Activities A GIS Multi Criteria Evaluation based on an MSF Humanitarian Mission in Cameroon (2016).

51. *Gezahagn Negash Seboka:* Spatial Assessment of NDVI as an Indicator of Desertification in Ethiopia using Remote Sensing and GIS (2016).

52. *Holly Buhler:* Evaluation of Interfacility Medical Transport Journey Times in Southeastern British Columbia. (2016).

53. *Lars Ole Grottenberg*: Assessing the ability to share spatial data between emergency management organisations in the High North (2016).

54. *Sean Grant:* The Right Tree in the Right Place: Using GIS to Maximize the Net Benefits from Urban Forests (2016).

55. *Irshad Jamal:* Multi-Criteria GIS Analysis for School Site Selection in Gorno-Badakhshan Autonomous Oblast, Tajikistan (2016).

56. *Fulgencio Sanmartín:* Wisdom-volkano: A novel tool based on open GIS and time-series visualization to analyse and share volcanic data (2016).

57. *Nezha Acil:* Remote sensing-based monitoring of snow cover dynamics and its influence on vegetation growth in the Middle Atlas Mountains (2016).

58. *Julia Hjalmarsson:* A Weighty Issue: Estimation of Fire Size with Geographically Weighted Logistic Regression (2016).

59. *Mathewos Tamiru Amato:* Using multi-criteria evaluation and GIS for chronic food and nutrition insecurity indicators analysis in Ethiopia (2016).

60. *Karim Alaa El Din Mohamed Soliman El Attar:* Bicycling Suitability in Downtown, Cairo, Egypt (2016).

61. *Gilbert Akol Echelai:* Asset Management: Integrating GIS as a Decision Support Tool in Meter Management in National Water and Sewerage Corporation (2016).

62. *Terje Slinning:* Analytic comparison of multibeam echo soundings (2016).

63. *Gréta Hlín Sveinsdóttir:* GIS-based MCDA for decision support: A framework for wind farm siting in Iceland (2017).

64. *Jonas Sjögren:* Consequences of a flood in Kristianstad, Sweden: A GIS-based analysis of impacts on important societal functions (2017).

65. *Nadine Raska:* 3D geologic subsurface modelling within the Mackenzie Plain, Northwest Territories, Canada (2017).

66. *Panagiotis Symeonidis*: Study of spatial and temporal variation of atmospheric optical parameters and their relation with PM 2.5 concentration over Europe using GIS technologies (2017).

67. *Michaela Bobeck:* A GIS-based Multi-Criteria Decision Analysis of Wind Farm Site Suitability in New South Wales, Australia, from a Sustainable Development Perspective (2017).

68. *Raghdaa Eissa*: Developing a GIS Model for the Assessment of Outdoor Recreational Facilities in New Cities Case Study: Tenth of Ramadan City, Egypt (2017).

69. *Zahra Khais Shahid*: Biofuel plantations and isoprene emissions in Svea and Götaland (2017).

70. *Mirza Amir Liaquat Baig*: Using geographical information systems in epidemiology: Mapping and analyzing occurrence of diarrhea in urban - residential area of Islamabad, Pakistan (2017).

71. *Joakim Jörwall*: Quantitative model of Present and Future well-being in the EU-28: A spatial Multi-Criteria Evaluation of socioeconomic and climatic comfort factors (2017).

72. *Elin Haettner*: Energy Poverty in the Dublin Region: Modelling Geographies of Risk (2017).

73. *Harry Eriksson*: Geochemistry of stream plants and its statistical relations to soil- and bedrock geology, slope directions and till geochemistry. A GIS-analysis of small catchments in northern Sweden (2017).

74. *Daniel Gardevärn:* PPGIS and Public meetings – An evaluation of public participation methods for urban planning (2017).

75. *Kim Friberg:* Sensitivity Analysis and Calibration of Multi Energy Balance Land Surface Model Parameters (2017).

76. *Viktor Svanerud:* Taking the bus to the park? A study of accessibility to green areas in Gothenburg through different modes of transport (2017).

77. *Lisa-Gaye Greene*: Deadly Designs: The Impact of Road Design on Road Crash Patterns along Jamaica's North Coast Highway (2017).

78. *Katarina Jemec Parker*: Spatial and temporal analysis of fecal indicator bacteria concentrations in beach water in San Diego, California (2017).

79. *Angela Kabiru*: An Exploratory Study of Middle Stone Age and Later Stone Age Site Locations in Kenya's Central Rift Valley Using Landscape Analysis: A GIS Approach (2017).

80. *Kristean Björkmann*: Subjective Well-Being and Environment: A GIS-Based Analysis (2018).

81. *Williams Erhunmonmen Ojo*: Measuring spatial accessibility to healthcare for people living with HIV-AIDS in southern Nigeria (2018).

82. *Daniel Assefa*: Developing Data Extraction and Dynamic Data Visualization (Styling) Modules for Web GIS Risk Assessment System (WGRAS). (2018).

83. *Adela Nistora*: Inundation scenarios in a changing climate: assessing potential impacts of sea-level rise on the coast of South-East England (2018).

84. *Marc Seliger*: Thirsty landscapes - Investigating growing irrigation water consumption and potential conservation measures within Utah's largest master-planned community: Daybreak (2018).

85. *Luka Jovičić*: Spatial Data Harmonisation in Regional Context in Accordance with INSPIRE Implementing Rules (2018).

86. *Christina Kourdounouli*: Analysis of Urban Ecosystem Condition Indicators for the Large Urban Zones and City Cores in EU (2018).

87. *Jeremy Azzopardi*: Effect of distance measures and feature representations on distance-based accessibility measures (2018).

88. *Patrick Kabatha*: An open source web GIS tool for analysis and visualization of elephant GPS telemetry data, alongside environmental and anthropogenic variables (2018).

89. *Richard Alphonce Giliba*: Effects of Climate Change on Potential Geographical Distribution of Prunus africana (African cherry) in the Eastern Arc Mountain Forests of Tanzania (2018).

90. *Eiður Kristinn Eiðsson*: Transformation and linking of authoritative multi-scale geodata for the Semantic Web: A case study of Swedish national building data sets (2018).

91. *Niamh Harty*: HOP!: a PGIS and citizen science approach to monitoring the condition of upland paths (2018).

92. *José Estuardo Jara Alvear*: Solar photovoltaic potential to complement hydropower in Ecuador: A GIS-based framework of analysis (2018).

93. *Brendan O'Neill*: Multicriteria Site Suitability for Algal Biofuel Production Facilities (2018).

94. *Roman Spataru*: Spatial-temporal GIS analysis in public health – a case study of polio disease (2018).

95. *Alicja Miodońska*: Assessing evolution of ice caps in Suðurland, Iceland, in years 1986 - 2014, using multispectral satellite imagery (2019).

96. *Dennis Lindell Schettini*: A Spatial Analysis of Homicide Crime's Distribution and Association with Deprivation in Stockholm Between 2010-2017 (2019).

97. *Damiano Vesentini*: The Po Delta Biosphere Reserve: Management challenges and priorities deriving from anthropogenic pressure and sea level rise (2019).

98. *Emilie Arnesten*: Impacts of future sea level rise and high water on roads, railways and environmental objects: a GIS analysis of the potential effects of increasing sea levels and highest projected high water in Scania, Sweden (2019).

99. *Syed Muhammad Amir Raza*: Comparison of geospatial support in RDF stores: Evaluation for ICOS Carbon Portal metadata (2019).

100. *Hemin Tofiq*: Investigating the accuracy of Digital Elevation Models from UAV images in areas with low contrast: A sandy beach as a case study (2019).

101. *Evangelos Vafeiadis*: Exploring the distribution of accessibility by public transport using spatial analysis. A case study for retail concentrations and public hospitals in Athens (2019).

102. *Milan Sekulic*: Multi-Criteria GIS modelling for optimal alignment of roadway by-passes in the Tlokweng Planning Area, Botswana (2019).

103. *Ingrid Piirisaar*: A multi-criteria GIS analysis for siting of utility-scale photovoltaic solar plants in county Kilkenny, Ireland (2019).

104. *Nigel Fox*: Plant phenology and climate change: possible effect on the onset of various wild plant species' first flowering day in the UK (2019).

105. *Gunnar Hesch*: Linking conflict events and cropland development in Afghanistan, 2001 to 2011, using MODIS land cover data and Uppsala Conflict Data Programme (2019).

106. *Elijah Njoku*: Analysis of spatial-temporal pattern of Land Surface Temperature (LST) due to NDVI and elevation in Ilorin, Nigeria (2019).

107. *Katalin Bunyevácz*: Development of a GIS methodology to evaluate informal urban green areas for inclusion in a community governance program (2019).

108. *Paul dos Santos*: Automating synthetic trip data generation for an agent-based simulation of urban mobility (2019).

109. *Robert O' Dwyer*: Land cover changes in Southern Sweden from the mid-Holocene to present day: Insights for ecosystem service assessments (2019).

110. *Daniel Klingmyr*: Global scale patterns and trends in tropospheric NO2 concentrations (2019).

111. *Marwa Farouk Elkabbany*: Sea Level Rise Vulnerability Assessment for Abu Dhabi, United Arab Emirates (2019).

112. *Jip Jan van Zoonen*: Aspects of Error Quantification and Evaluation in Digital Elevation Models for Glacier Surfaces (2020).

113. *Georgios Efthymiou*: The use of bicycles in a mid-sized city – benefits and obstacles identified using a questionnaire and GIS (2020).

114. *Haruna Olayiwola Jimoh*: Assessment of Urban Sprawl in MOWE/IBAFO Axis of Ogun State using GIS Capabilities (2020).

115. *Nikolaos Barmpas Zachariadis*: Development of an iOS, Augmented Reality for disaster management (2020).

116. *Ida Storm*: ICOS Atmospheric Stations: Spatial Characterization of CO2 Footprint Areas and Evaluating the Uncertainties of Modelled CO2 Concentrations (2020).

117. *Alon Zuta*: Evaluation of water stress mapping methods in vineyards using airborne thermal imaging (2020).

118. *Marcus Eriksson*: Evaluating structural landscape development in the municipality Upplands-Bro, using landscape metrics indices (2020).

119. *Ane Rahbek Vierø*: Connectivity for Cyclists? A Network Analysis of Copenhagen's Bike Lanes (2020).

120. *Cecilia Baggini*: Changes in habitat suitability for three declining Anatidae species in saltmarshes on the Mersey estuary, North-West England (2020).

121. *Bakrad Balabanian*: Transportation and Its Effect on Student Performance (2020).

122. *Ali Al Farid*: Knowledge and Data Driven Approaches for Hydrocarbon Microseepage Characterizations: An Application of Satellite Remote Sensing (2020).

123. *Bartlomiej Kolodziejczyk*: Distribution Modelling of Gene Drive-Modified Mosquitoes and Their Effects on Wild Populations (2020).

124. *Alexis Cazorla*: Decreasing organic nitrogen concentrations in European water bodies - links to organic carbon trends and land cover (2020).

125. *Kharid Mwakoba*: Remote sensing analysis of land cover/use conditions of community-based wildlife conservation areas in Tanzania (2021).

126. *Chinatsu Endo*: Remote Sensing Based Pre-Season Yellow Rust Early Warning in Oromia, Ethiopia (2021).

127. *Berit Mohr*: Using remote sensing and land abandonment as a proxy for long-term human out-migration. A Case Study: Al-Hassakeh Governorate, Syria (2021).

128. *Kanchana Nirmali Bandaranayake*: Considering future precipitation in delineation locations for water storage systems - Case study Sri Lanka (2021).

129. *Emma Bylund*: Dynamics of net primary production and food availability in the aftermath of the 2004 and 2007 desert locust outbreaks in Niger and Yemen (2021).

130. *Shawn Pace*: Urban infrastructure inundation risk from permanent sea-level rise scenarios in London (UK), Bangkok (Thailand) and Mumbai (India): A comparative analysis (2021).

131. *Oskar Evert Johansson*: The hydrodynamic impacts of Estuarine Oyster reefs, and the application of drone technology to this study (2021).

132. *Pritam Kumarsingh*: A Case Study to develop and test GIS/SDSS methods to assess the production capacity of a Cocoa Site in Trinidad and Tobago (2021).

133. *Muhammad Imran Khan*: Property Tax Mapping and Assessment using GIS (2021).

134. *Domna Kanari*: Mining geosocial data from Flickr to explore tourism patterns: The case study of Athens (2021).

135. *Mona Tykesson Klubien*: Livestock-MRSA in Danish pig farms (2021).

136. *Ove Njøten*: Comparing radar satellites. Use of Sentinel-1 leads to an increase in oil spill alerts in Norwegian waters (2021).

137. *Panagiotis Patrinos*: Change of heating fuel consumption patterns produced by the economic crisis in Greece (2021).

138. *Lukasz Langowski*: Assessing the suitability of using Sentinel-1A SAR multi-temporal imagery to detect fallow periods between rice crops (2021).

139. *Jonas Tillman*: Perception accuracy and user acceptance of legend designs for opacity data mapping in GIS (2022).

140. *Gabriela Olekszyk*: ALS (Airborne LIDAR) accuracy: Can potential low data quality of ground points be modelled/detected? Case study of 2016 LIDAR capture over Auckland, New Zealand (2022).

141. *Luke Aspland*: Weights of Evidence Predictive Modelling in Archaeology (2022).

142. *Luís Fareleira Gomes*: The influence of climate, population density, tree species and land cover on fire pattern in mainland Portugal (2022).

143. *Andreas Eriksson*: Mapping Fire Salamander (Salamandra salamandra) Habitat Suitability in Baden-Württemberg with Multi-Temporal Sentinel-1 and Sentinel-2 Imagery (2022).

144. *Lisbet Hougaard Baklid*: Geographical expansion rate of a brown bear population in Fennoscandia and the factors explaining the directional variations (2022).

145. *Victoria Persson*: Mussels in deep water with climate change: Spatial distribution of mussel (Mytilus galloprovincialis) growth offshore in the French Mediterranean with respect to climate change scenario RCP 8.5 Long Term and Integrated Multi-Trophic Aquaculture (IMTA) using Dynamic Energy Budget (DEB) modelling (2022).

146. *Benjamin Bernard Fabien Gérard Borgeais*: Implementing a multi-criteria GIS analysis and predictive modelling to locate Upper Palaeolithic decorated caves in the Périgord noir, France (2022).

147. *Bernat Dorado-Guerrero*: Assessing the impact of post-fire restoration interventions using spectral vegetation indices: A case study in El Bruc, Spain (2022).

148. *Ignatius Gabriel Aloysius Maria Perera*: The Influence of Natural Radon Occurrence on the Severity of the COVID-19 Pandemic in Germany: A Spatial Analysis (2022).

149. *Mark Overton*: An Analysis of Spatially-enabled Mobile Decision Support Systems in a Collaborative Decision-Making Environment (2022).

150. *Viggo Lunde*: Analysing methods for visualizing time-series datasets in open-source web mapping (2022).

151. *Johan Viscarra Hansson*: Distribution Analysis of Impatiens glandulifera in Kronoberg County and a Pest Risk Map for Alvesta Municipality (2022).

152. *Vincenzo Poppiti*: GIS and Tourism: Developing strategies for new touristic flows after the Covid-19 pandemic (2022).

153. *Henrik Hagelin*: Wildfire growth modelling in Sweden - A suitability assessment of available data (2023).

154. *Gabriel Romeo Ferriols Pavico*: Where there is road, there is fire (influence): An exploratory study on the influence of roads in the spatial patterns of Swedish wildfires of 2018 (2023).

155. *Colin Robert Potter*: Using a GIS to enable an economic, land use and energy output comparison between small wind powered turbines and large-scale wind farms: the case of Oslo, Norway (2023).

156. *Krystyna Muszel*: Impact of Sea Surface Temperature and Salinity on Phytoplankton blooms phenology in the North Sea (2023).